JACS
JOURNAL OF THE AMERICAN CHEMICAL SOCIETY
Article
pubs.acs.org/JACS

Unravelling the Mechanism of Basic Aqueous Methanol Dehydrogenation Catalyzed by Ru−PNP Pincer Complexes

Elisabetta Alberico,[⊥,†,‡] Alastair J. J. Lennox,[⊥,†] Lydia K. Vogt,[†] Haijun Jiao,[†] Wolfgang Baumann,[†] Hans-Joachim Drexler,[†] Martin Nielsen,[§] Anke Spannenberg,[†] Marek P. Checinski,[∥] Henrik Junge,[†] and Matthias Beller*[,†]

[†]Leibniz Institute for Catalysis, University of Rostock, Albert Einstein-Straße 29a, 18059 Rostock, Germany

[‡]Istituto di Chimica Biomolecolare, Consiglio Nazionale delle Ricerche, tr. La Crucca 3, 07100 Sassari, Italy

[§]Centre for Catalysis and Sustainable Chemistry, Department of Chemistry, Technical University of Denmark, Kemitorvet 207, 2800 Kgs. Lyngby, Denmark

[∥]CreativeQuantum GmbH, Wegedornstraße 32, 12524 Berlin, Germany

Supporting Information

ABSTRACT: Ruthenium PNP complex **1a** (RuH(CO)Cl-(HN(C_2H_4P*i*-Pr$_2$)$_2$)) represents a state-of-the-art catalyst for low-temperature (<100 °C) aqueous methanol dehydrogenation to H_2 and CO_2. Herein, we describe an investigation that combines experiment, spectroscopy, and theory to provide a mechanistic rationale for this process. During catalysis, the presence of two anionic resting states was revealed, Ru−dihydride (3^-) and Ru−monohydride (4^-) that are deprotonated at nitrogen in the pincer ligand backbone. DFT calculations showed that O- and CH- coordination modes of methoxide to ruthenium compete, and form complexes 4^- and 3^-, respectively. Not only does the reaction rate increase with increasing KOH, but the ratio of $3^-/4^-$ increases, demonstrating that the "inner-sphere" C—H cleavage, via C—H coordination of methoxide to Ru, is promoted by base. Protonation of 3^- liberates H_2 gas and formaldehyde, the latter of which is rapidly consumed by KOH to give the corresponding gem-diolate and provides the overall driving force for the reaction. Full MeOH reforming is achieved through the corresponding steps that start from the gem-diolate and formate. Theoretical studies into the mechanism of the catalyst **Me-1a** (*N*-methylated **1a**) revealed that C—H coordination to Ru sets-up C—H cleavage and hydride delivery; a process that is also promoted by base, as observed experimentally. However, in this case, Ru−dihydride **Me-3** is much more stable to protonation and can even be observed under neutral conditions. The greater stability of **Me-3** rationalizes the lower rates of **Me-1a** compared to **1a**, and also explains why the reaction rate then drops with increasing KOH concentration.

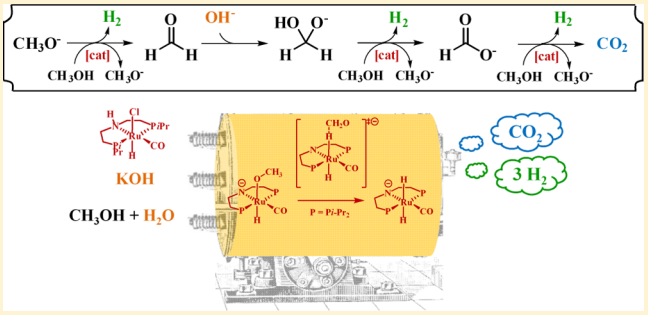

INTRODUCTION

Concerns over depleting fossil fuels and the negative effects of increasing CO_2 emissions have stimulated the search for more sustainable energy sources.[1] Hydrogen has been identified as a possible alternative source.[2] Its high-energy combustion or use in fuel cells[3] generates water as the sole byproduct. However, the physical and chemical properties of H_2 gas do not render it an ideal energy vector. With a limited volumetric energy density, it must be either compressed at very high pressure (350−700 bar) or liquefied at very low temperature (−253 °C). In addition, H_2 is highly flammable and can diffuse through several metals and materials.[2] Thus, the chemical storage of H_2 in solid or liquid compounds is currently intensively investigated.[4] In particular, alcohols[5] constitute suitable H_2 carriers. Among these, methanol is considered to be the most viable option,[6] as it is a liquid at room temperature and has a comparatively high H_2 content (12.6 wt %), which can be released through steam reforming, Scheme 1A.[7]

Scheme 1. Methanol Steam Reforming (A) and Liquid-Phase Dehydrogenation (B)

A

$$CH_3OH(g) + H_2O(g) \longrightarrow 3H_2(g) + CO_2(g) \quad \Delta H^\circ_{298} = 53.3\ kJmol^{-1},\ \Delta G^\circ_{298} = 0.6\ kJmol^{-1}$$

B

$$CH_3OH(l) + H_2O(l) \longrightarrow 3H_2(g) + CO_2(g) \quad \Delta H^\circ_{298} = 130.7\ kJmol^{-1},\ \Delta G^\circ_{298} = 8.9\ kJmol^{-1}$$

In general, this reaction is performed using either copper-based (CuO/ZnO/Al_2O_3) or group 8−10 metal-based (Pd−Zn alloys) heterogeneous catalysts that operate at high temperature (200−300 °C).[8] Although highly active and selective, the copper-based catalysts are pyrophoric and deactivate due to metal particle sintering above 300 °C. Moreover, through a

Received: June 3, 2016
Published: October 19, 2016

DOI: 10.1021/jacs.6b05692
J. Am. Chem. Soc. 2016, 138, 14890−14904

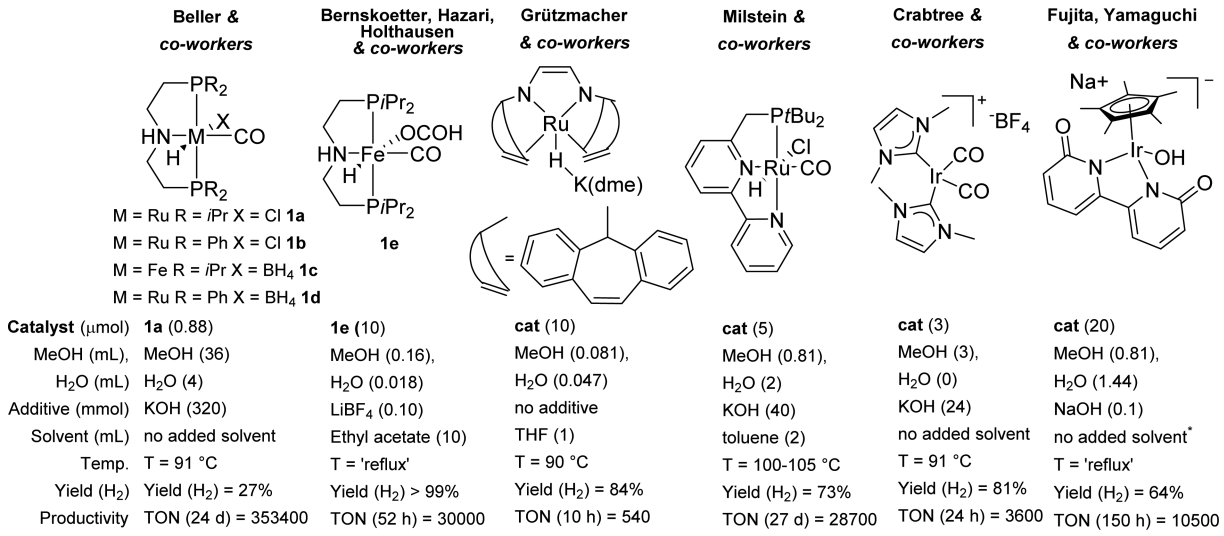

Figure 1. A comparison of a selection of catalysts able to engender full methanol dehydrogenation. *Syringe-pump addition of MeOH/H_2O/NaOH (0.6/0.6/0.001 mmol h^{-1}).

reverse water−gas-shift reaction, the high temperatures favor CO formation, which is incompatible with current fuel cell technologies.

In efforts toward tackling these problems, we recently demonstrated the first low temperature dehydrogenation of aqueous methanol to H_2 and CO_2 with almost no trace of CO contamination, Scheme 1B.[9] First reported for acceptorless dehydrogenation of secondary alcohols,[10a,b] we identified the homogeneous ruthenium-based PNP−pincer complex **1a**, Figure 1, suitable for the aqueous reforming of methanol under basic conditions.[9] Originally developed for ester hydrogenation,[10c,d] catalyst **1b** was also found to facilitate this transformation. Notably, employing <1 ppm of **1a** below 100 °C TOFs up to =4720 h^{-1} were observed (40 mL MeOH, 8 M KOH, 1.58 μmol **1a**). This complex proved to be highly stable (23 days) affording TONs > 350 000 (40 mL MeOH:H_2O (9:1), 8 M KOH, 0.88 μmol **1a**), which represents the most active and productive low temperature methanol reforming system developed to date. Since then, other catalysts based on Ru[11] and Fe[12] appeared in the literature, Figure 1, clearly illustrating the potential for this strategy. Multidentate pincer ligands are common to these complexes, as they secure high thermal stability and are uniquely involved in the catalytic cycle. These "non-innocent"[13] ligands participate in metal−ligand bifunctional catalysis.[14] Other catalysts that do not bear pincer ligands have also been reported, including Grützmacher's and co-workers',[11a] which engages in ligand cooperativity,[15] and two others based on iridium,[16,17] which, like the catalysts used by us, are active without additional solvent.

Complete methanol reforming requires a catalyst that can facilitate three consecutive steps, Scheme 2. The first H_2 release originates from the dehydrogenation of methanol to formaldehyde. Subsequent reaction with water gives a gem-diol, which liberates the second equivalent of H_2 upon its dehydrogenation to formic acid. Final dehydrogenation to CO_2 releases the third H_2 molecule.

Through a qualitative analysis of the data, a common mechanism for all three steps using **1a** was proposed, involving an "outer-sphere" concerted association of methanol to the coordinatively unsaturated amido complex **2**, Scheme 3.

Scheme 2. Three Steps for Methanol Dehydrogenation

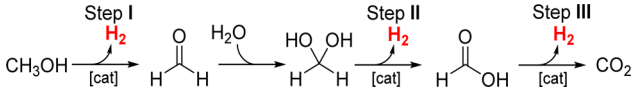

Scheme 3. Previously Proposed Direct Outer-Sphere Addition to Form Intermediate 3 (P = P*i*-Pr$_2$)

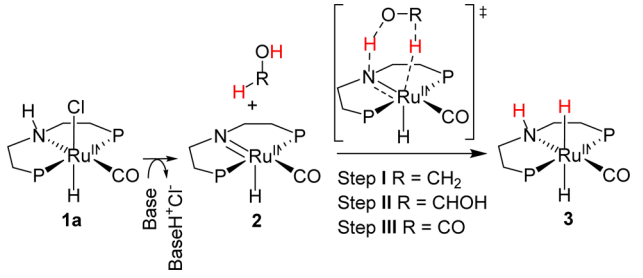

Transfer of a proton to nitrogen and a hydride to Ru generates dihydride complex **3**, from which a solvent assisted[18] liberation of H_2 gas ensues. Support for this hypothesis came from DFT calculations by Yang,[19a] according to whom the key C—H cleavage step, Scheme 3, is a stepwise process, wherein hydride is transferred from an uncoordinated methoxide to the cationic Ru center. This proposal was supported by Lei and co-workers, who suggested that the dehydrogenation of formate could occur either via an outer or inner sphere mechanism.[19b] The outer-sphere mechanism was proposed to proceed via the same transition state to our prior suggestions, Scheme 3, whereas the inner sphere followed a nonclassical hydride elimination, much like that proposed by Milstein and co-workers.[20] Despite providing considerably different absolute energetics for each step, both theoretical studies agree on the relative free-energy barriers of the three consecutive steps; with gem-diol and formic acid dehydrogenation being the most and least facile step, respectively. This prediction is in line with experimental observations,[9] as formaldehyde/gemdiol escape detection, while formate steadily builds up in solution (^{1}H NMR).

DOI: 10.1021/jacs.6b05692
J. Am. Chem. Soc. 2016, 138, 14890−14904

Most catalysts developed so far for methanol dehydrogenation require either a base or acid additive to secure significant activity. A Lewis acid promotes precatalyst decarboxylation in **1e**;[12b] however, base is required for those described by our group (**1a**–**d**),[9,12a] as well as Milstein and co-workers[11c] and Fujita/Yamaguchi[17] and co-workers. Notably, present mechanistic and theoretical investigations of the state-of-the-art catalyst **1a** do not provide a reasonable rationale for the necessity of the very high base concentrations employed. Herein, we report for the first time on a detailed mechanistic investigation of this process employing a mixture of experimental, spectroscopic and theoretical tools.

RESULTS AND DISCUSSION

Inner-Sphere vs Outer-Sphere. We began by investigating the notion of an "outer-sphere" mechanism in order to establish whether the ligand is truly noninnocent. Replacing H—N with Me—N on the backbone is a common strategy to probe ligand cooperativity. Metal complexes, e.g., Ru,[21] Fe,[22] Co,[23] and Ni[24] with the aliphatic pincer ligands (HN-$(CH_2CH_2PR_2)_2$, R = alkyl or Ph) have been applied to the hydrogenation of CO_2,[21a,22b] bicarbonate,[21b] cyclic carbonates,[21f] nitriles,[21c,22c] esters,[22d] ketones,[23b] alkenes,[22a,23b] and *N*-heterocycles.[23d] Use of the corresponding *N*-methylated catalysts results in no activity in all cases of hydrogenation,[21a,c,f,22a−c,23b,d] except that of bicarbonate,[21b] CO_2 promoted by Fe−MePNP complexes in the presence of Lewis acid cocatalysts,[22b] and olefins catalyzed by Co complexes.[23b,6] However, *N*-methylation of the ligand in Co and Ru complexes furnish good yields in the dehydrogenation of alcohols[21d,22e,23b] and *N*-heterocycles[23d] as well as in the transfer hydrogenation of ketones,[23c] imines,[23c] and olefins.[23e] However, rates of these reactions were not measured and cannot be compared to those using the nonmethylated catalysts. In ammonia-borane dehydrocoupling, the *N*-methylated Ru complex results in a rate that is 2 orders of magnitude lower than that obtained with the corresponding N—H complex.[21e] Gas phase calculations of this system predicted the same general mechanism, but with higher energy barriers.

In order to probe bifunctional reactivity of **1a**, we prepared the corresponding *N*-methylated complex (**Me-1a**) (see Supporting Information, SI 2.1). The complex was obtained as a mixture of two isomers **Me-1a** (80%) and **Me-1a′** (20%), both containing equivalent phosphorus donors (^{31}P NMR (C_6D_6): **Me-1a** δ = 71.05 and **Me-1a′** δ = 73.63) (see SI 2.1). The relative $^2J_{HP}$ coupling constants of the corresponding triplet in the ^{1}H NMR spectrum (^{1}H NMR (C_6D_6): **Me-1a** δ = −15.33 ($^2J_{HP}$ = 18.2 Hz), **Me-1a′** δ = −15.25 ($^2J_{HP}$ = 18.6 Hz)) indicate the hydride is cis to both P atoms. The two isomers are due to the relative orientation of methyl: syn or anti to the hydride on Ru, and have very similar chemical shifts. X-ray analysis from a single crystal was consistent with NMR and confirmed the CO to be trans to the nitrogen of the meridional coordinated PNP ligand, Figure 2.

Unfortunately, it was not possible to correlate the solid structure to one of the two isomers in solution and there was no evidence of a spatially relevant cross-peak in the ^{1}H NOESY spectrum. However, both isomers were computationally located: *syn*-**Me-1a** is more stable than *anti*-**Me-1a** by 0.50 kcal mol^{-1}, corresponding to an isomeric ratio of 70 to 30, which is in good agreement with that observed experimentally (80:20). When the catalytic activity of **Me-1a** was tested under the optimized dehydrogenation conditions, Figure 3 (see SI 2.2), we were surprised to observe that the rate was only 2.4 times lower than using **1a**. Considering a difference of 2 orders of magnitude was observed for catalysts undergoing the same mechanism in the case of ammonia-borane dehydrocoupling,[21e] it was conceivable that **1a** and **Me-1a** followed the same mechanism.

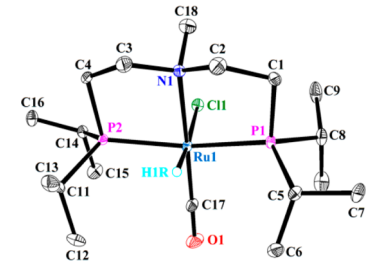

Figure 2. ORTEP view of *anti*-**Me-1a** with thermal ellipsoids drawn at the 30% probability level. H atoms (except H1R) are omitted for clarity.

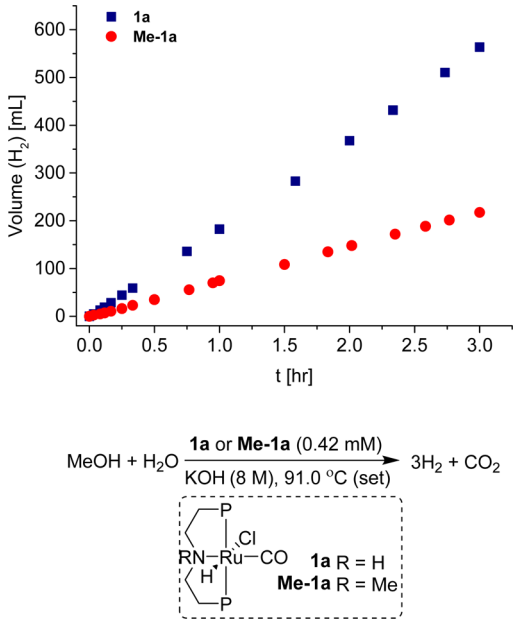

Figure 3. A comparison of rates in the aqueous methanol reforming promoted by parent catalyst **1a** and its *N*-methylated derivative **Me-1a**. *P* = P*i*-Pr$_2$.

In order to further understand this unexpected reactivity, we measured the kinetic isotope effects (KIEs)[25] with each catalyst, **1a** and **Me-1a**, using both fully deuterated and undeuterated solvents and base (see SI 2.3). A striking difference in the KIEs between the two catalysts was observed. **1a** provided a substantial isotope rate ratio of 7.07 compared to only 1.76 recorded with **Me-1a**, Scheme 4. It is nontrivial to directly assess the implications of these values, as the rate measure-

Scheme 4. KIE Measurements for Catalyst 1a and Me-1a

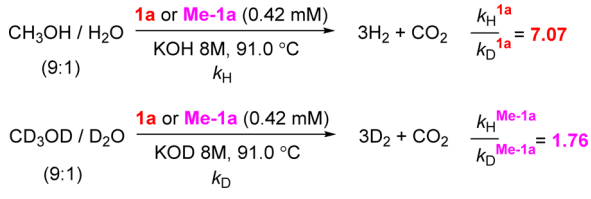

DOI: 10.1021/jacs.6b05692
J. Am. Chem. Soc. 2016, 138, 14890−14904

ments are from a product (H_2) that evolves over three separate reactions, Scheme 2. Absolute rates before the steady state stage are interconnected, because the product of each step is the starting material of the following one. Once at steady-state and "real" reforming proceeds, rates for each step do not change, however, the KIE is still a composite from all steps and is therefore difficult to disentangle.

The evolution of gas is observed to proceed through pseudo zero order kinetics, Figure 3. At the levels of conversion reached over the time periods studied, the concentrations of MeOH, water and catalyst remain effectively constant. Thus, additional information from the decay curves of limiting reagents or intermediates cannot be gathered under normal catalytic conditions.[26] The TOF decreased with increasing catalyst loading (see SI 2.4), an interesting effect similarly observed by Gusev and co-workers[21g] and more recently by Gauvin/Dumeignil and co-workers.[21h] Indeed, the reaction order with respect to catalyst was measured to be below 1. These data may be attributed to an off-cycle Ru-dimerization at higher loadings, although no such intermediates could be detected by ^{31}P NMR. Alternatively, the mass-transfer of H_2 out of the system might limit the rate at higher Ru-loadings, as the reaction is reversible and hydrogenation processes can occur at higher H_2 concentrations (pressures), vide infra. Providing support for this hypothesis, the rate of reaction was found to be dependent on the stirring rate (see SI 2.5), as also observed by Gauvin/Dumeignil and co-workers.[21h] Deuteration decreased the reaction rate 7-fold in the case of **1a**, but not even 2-fold in the case of **Me-1a**. Thus, despite **Me-1a** being active, the magnitude of the KIE difference implies different operating mechanisms for the two catalysts. Apparently for **Me-1a**, in contrast to **1a**, the turnover limiting step(s) does not significantly involve the cleavage of an X—H (X = C, O, Ru) bond.

Temperature and Base Dependency Measurements. During reaction optimization, we observed that high base concentrations increased the catalytic activity significantly. An optimal operational pH has also been reported for bifunctional Ru catalyzed hydrogenation[27a−c] and transfer hydrogenation[27b,d] of ketones. Initially, we speculated that the increased activity was due to the inflated temperature over the boiling point of the solvent, which could be reached due to the salt-effect from the high KOH concentration. To test this, we attempted to replace KOH with innocent salts (e.g., KNO_3, KPF_6) to effect the same temperature increase. However, all the salts tested did not provide a homogeneous solution and so it could not be fairly examined this way. In addition, mixing methanol with higher boiling point cosolvents, e.g., *N*-methylpyrrolidine or *t*-BuOH, shut down the reactivity. Thus, we examined the rate of methanol dehydrogenation systematically at a range of lower temperatures (50−90 °C). The average rate measured over a 3 h period increased exponentially with temperature, and produced a linear Arrhenius plot, Figure 4.

To further understand the influence of base, we measured rates at different KOH concentrations at constant temperature. It was necessary to modify the setup, because at low concentrations of base it is not possible to raise the temperature above the boiling point of the solvent. Hence, we used an autoclave to which an overpressure was applied to increase the boiling point and to ensure the solvent remained in the liquid phase (see SI 1.2). However, hydrogen evolution was considerably lower than that observed using our original buret setup in an open system (see SI 1.1). Several control

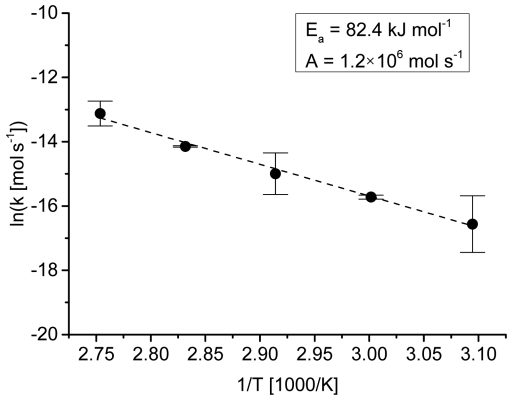

Figure 4. Arrhenius plot to show the dependency of activity on temperature for aqueous methanol reforming promoted by catalyst **1a**. Conditions: 8 M KOH, MeOH:H_2O (9:1, 10 mL), 4.2 μmol **1a**, 3 h.

reactions were undertaken that confirmed the attenuation to arise from the reverse reaction: specifically, H_2 and CO_2 inserting into catalytic intermediates (vide infra). This complication was controlled by leaking the evolved gas through a valve and retaining an over pressure of 0.6 bar (see SI 1.3). Despite providing lower rates than in an open vessel (TOF = 550 h^{-1} vs 1770 h^{-1}, 8 M KOH), this adjustment was sufficient to reach 90 °C without suffering from the strong attenuation observed with full pressurization. Using this modified setup, it was possible to measure the rate using 4−8 M KOH with both **1a** and **Me-1a** catalysts, albeit with an increased loading of **Me-1a.** To record the rates below 4 M KOH, it was necessary to decrease the temperature to 60 °C. At this temperature, the regular buret setup was employed (see SI 1.1). For catalyst **1a**, a first order dependence was observed at 60 °C, Figure 5. At 90

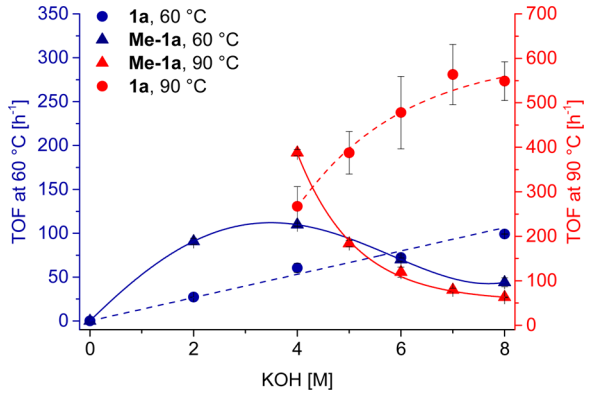

Figure 5. Influence of KOH concentration on the activity of catalysts **1a** and **Me-1a** in methanol reforming at 60 and 90 °C. Conditions at 60 °C: 10 mL MeOH:H_2O (9:1) and **1a** (8.41 μmol, blue dots) or **Me-1a** (8.41 μmol, blue triangles) using the "regular" buret setup. Conditions at 90 °C: 20 mL MeOH:H_2O (9:1) and **1a** (8.41 μmol, red dots) or **Me-1a** (16.82 μmol, red triangles) in a leaking autoclave set to an over pressure of 0.6 bar. Lines are solely a guide for the eye.

°C, saturation kinetics appears at KOH concentrations above 7 M, which may be due to the mass-transport limiting loss of H_2 from the system at high reaction rates, vide supra. For catalyst **Me-1a**, a peak in rate was observed at 4 M KOH, after which the rate dropped.

Stoichiometric Studies. To further deconvolute the mechanism, we prepared and characterized the reactivity of a

DOI: 10.1021/jacs.6b05692
J. Am. Chem. Soc. 2016, 138, 14890−14904

number of Ru complexes that are possible intermediates in the catalytic cycle.

Activation of 1a. **1a** was prepared following a published procedure,[10a] and, like **Me-1a**, was obtained as a mixture of two stereoisomers, *syn*-**1a** and *anti*-**1a**, which differ only in the relative orientation of the chloride ligand and the hydrogen on nitrogen. Both isomers are spectroscopically (^{1}H, ^{31}P NMR) similar, and have equivalent phosphorus donors indicated by singlet peaks (^{31}P{^{1}H} NMR (THF-d_8) *syn*-**1a** δ = 75.8 and *anti*-**1a** δ = 76.3) (see SI 3.1). The coupling constant, J_{HP}, of the hydride triplet in the ^{1}H NMR spectrum indicates a cis relationship to both phosphorus atoms (^{1}H NMR: *syn*-**1a** δ = −15.7 (J_{HP} = 19.2 Hz, RuH) and *anti*-**1a** δ = −16.0 (J_{HP} = 17.9 Hz, RuH)). Crystals suitable for X-ray analysis were obtained from the slow diffusion between a dilute diglyme/diethyl ether solution, Figure 6. The diffraction data allowed for independent

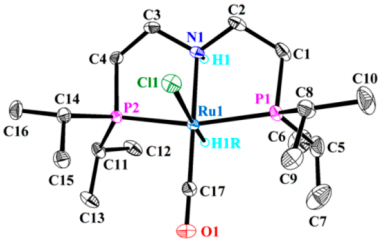

Figure 6. ORTEP view of *syn*-**1a** with thermal ellipsoids drawn at the 30% probability level. H atoms other than H1 and H1R are omitted for clarity.

location and refinement of both the hydride ligand and the hydrogen on nitrogen. The solid-state structure confirmed that the ligand is coordinated to Ru in a meridional fashion with CO ligated trans to nitrogen. The hydride is disposed cis to both phosphorus donors and also syn to the hydrogen on nitrogen, thereby confirming it to be *syn*-**1a**, which was shown to be the minor isomer that appears in solution (^{1}H NMR).[28] We also located both isomers computationally; in line with our NMR observations, *anti*-**1a** is more stable than *syn*-**1a** by 3.26 kcal mol^{-1}.

Dehydrochlorination of **1a** to Ru−amido **2** must occur before catalysis proceeds (Scheme 5). Initiation of this

Scheme 5. Generation of 2 by Dehydrochlorination of 1a with Base (P = P*i*-Pr$_2$)

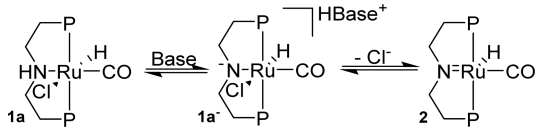

activation process by base was tested by treatment with 1 equiv of *t*-BuOK in diethyl ether. A yellow, air sensitive complex was formed, whose spectral properties are consistent with that of amido complex **2**, Scheme 5.[9] The two phosphorus donors of **2** are again equivalent, (^{31}P NMR (THF-d_8): δ = 93.8, one signal)), although the peak is shifted to a lower field than **1a**, consistent with a more deshielded P-nucleus. The hydride ligand is cis to both phosphorus atoms, as judged by the relative J_{HP} coupling constants in the triplet peak (^{1}H NMR (THF-d^8): δ = −19.0 (J_{HP} = 17.1 Hz)).[29] Crystals of **2** suitable for X-ray analysis were grown from *n*-heptane at −78 °C, Figure 7.[28] The Ru(II) complex **2** displays a Y-shaped distorted trigonal bipyramidal coordination geometry, where N1, H1R, and C17 (from the CO ligand) define the equatorial plane.

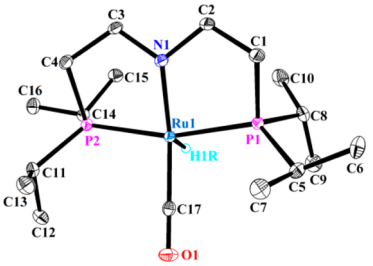

Figure 7. ORTEP view of **2** with thermal ellipsoids drawn at the 30% probability level. Hydrogen atoms other than H1R are omitted for clarity. The distortion from an ideal trigonal bipyramid arises from the small H1R—Ru—C17 angle (82.7(7)°) and the large H1R—Ru—N1 (120.4(7)°) and N1—Ru—C17 (156.89(6)°) angles. The N1—Ru distance (1.9985(12) Å) in **2** is considerably shorter than in *syn*-**1a** (2.1949(18) Å).[30]

HCl elimination from **1a** proceeds according to a dissociative conjugate base mechanism (Dcb mechanism).[31] Base abstracts the acidic proton on nitrogen to generate a stabilized anion, prompting chloride to leave and the formal formation of an N—Ru double bond. The lifetime of the anionic intermediate (**1a**$^-$) is too short for detection, indicating rapid chloride elimination. Coordination to Ru and the presence of the trans, strongly π-accepting, CO ligand, increase the acidity of the amino group. The reversibility of this activation mechanism was tested by employing a weaker base. Thus, *anti*-**1a** was treated with 1−3 equiv of triethylamine at room temperature in THF-d_8 and monitored by ^{1}H NMR (see SI 3.2). Indeed, isomerization between anti and syn was observed, demonstrating rapid reversibility in the process, Scheme 5. However, under catalytic conditions, the rate of methanol dehydrogenation was unaffected by a 10-fold excess of additional KCl (see SI 3.3), thus indicating the reverse process is kinetically irrelevant. **2** was also never observed in solution under catalytic-like conditions. In order to understand the reactivity of this highly sensitive complex, its interactions with methanol, water, and formic acid were examined under inert conditions.

Reactions of Complex 2. When 2 equiv of MeOH in THF-d_8 were added to amido complex **2** at room temperature, the characteristic bright yellow color instantly disappeared and two major complexes were observed (^{1}H and ^{31}P NMR), Scheme 6 (see SI 4.1). Under these aprotic conditions, dihydride complex **3** was detected (^{1}H and ^{31}P NMR, vide infra) and accounted for 54% of the total Ru content. The second major species (36%) identified was a monohydride species. The peak for this monohydride complex (^{1}H NMR

Scheme 6. Reaction of Amido Complex 2 with Methanol and the Equilibrium between the Products (P = P*i*-Pr$_2$)

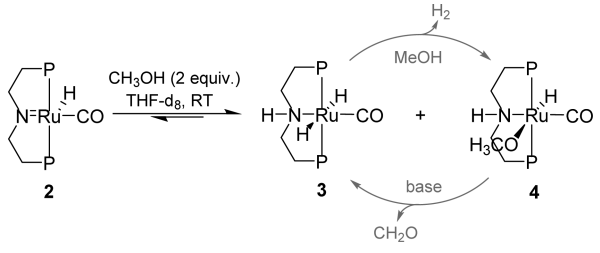

DOI: 10.1021/jacs.6b05692
J. Am. Chem. Soc. 2016, 138, 14890−14904

(THF-d_8): δ = −17.3 ($^2J_{HP}$ = 18.9 Hz))[32] suggests the hydride ligand is trans to a weak donor[33] and cis to the two equivalent phosphorus donors. This is consistent with formation of the Ru−methoxide complex (**4**); similar complexes have been detected in the hydrogenation of ketones.[27c−e,34] Gusev and co-workers have also observed an Ru−alkoxide complex in equilibrium with a Ru−dihydride complex.[10a] The methyl peaks of Ru-coordinated ^{13}C-enriched methoxide (Ru—O^{13}CH$_3$) and methanol (^{13}CH$_3$OH) appear as a single doublet in the room temperature ^{1}H NMR (see SI 4.1). When the solution was cooled, these peaks separated out into two well resolved doublets. Ru−alkoxide species can be stabilized by intramolecular hydrogen bonding with the backbone N—H,[27e] as well as intermolecular bonding with excess methanol.[35] To confirm the existence of a Ru—O bond, we treated the sample with CO_2 and rapidly detected a Ru−methylcarbonate complex, resulting from the formal insertion of CO_2 in the Ru—O bond (see SI 4.2). Only one isomer was formed, in which the backbone N—H was strongly shifted to lower fields due to hydrogen bonding to the carbonate (^{1}H NMR, THF-d_8, δ = 7.6 (b)). **4** was too unstable to be isolated, as it reverted back to Ru−amido **2** upon solvent removal and reduced pressure. This seemingly very facile addition/elimination process is supported by DFT. The addition of methanol across the N—Ru bond [**2** + CH_3OH = **4**] is only slightly endergonic (0.89 kcal mol^{-1}) and the Gibbs free energy barrier is 4.41 kcal mol^{-1}, Scheme 7. This is in line with the experimental observations and confirms the reaction reversibility.

Scheme 7. B3PW91-Generated Gibbs Free-Energies (kcal mol^{-1}) of Protic Species Addition to Ru−Amido Complex 2 (P = P*i*-Pr$_2$)

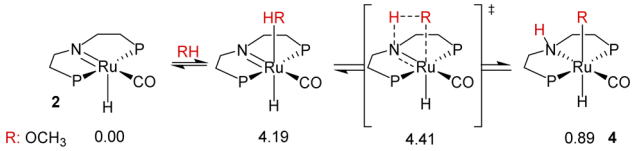

R: OCH_3	0.00	4.19	4.41	0.89	**4**
R: OH	0.00	2.74	2.65	0.25	**5**
R: H	0.00	9.37	18.76	-2.31	**3**
R: OCH_2OH	0.00	7.20	3.60	2.61 (-1.50)	**7**
R: OOCH	0.00	not located	not located	-19.71	**6**

An apparent equilibrium exists between the corresponding mono and dihydride Ru complexes, Scheme 6, which is affected by the addition of base or protic species. Hence, when NaOMe was added to **2**, only **3** was detected.[36] In addition, when 2 equiv *t*-BuOK were added to a mixture of **4** and **3**, all material was converted to **3**, consistent with a single turnover in the catalytic cycle, vide infra. Conversely, MeOH addition induced the conversion of **3** to **4**; after 50 equiv were added, and 78% of **4** had formed from protonation of **3** and release of H_2 gas. We calculated the free energy change of the studied reactions, Scheme 6. The reaction of **2** with methanol to **3** and formaldehyde [**2** + CH_3OH = **3** + CH_2O] is endergonic by 11.4 kcal mol^{-1}, which is close to that calculated by Yang (9.2 kcal mol^{-1})[19a] and Lei and co-workers (11.8 kcal mol^{-1}).[19b] The driving force for this reaction under these conditions (THF, room temperature) should be the formation of gaseous formaldehyde (bp = −21 °C). Formaldehyde dissociation ($\Delta G°$ = −2.45 kcal mol^{-1}) and trimerization ($\Delta G°$ = −2.96 kcal mol^{-1}) pathways were also computed but could not account for the energy shortfall. The exchange reaction between **3** and **4** [**3** + CH_3OH = **4** + H_2], is endergonic by 3.19 kcal mol^{-1}. The driving force in this case should be the formation of gaseous H_2.

The addition of gem-diol to **2** was calculated to be exergonic by 1.50 kcal mol^{-1} or endergonic by 2.61 kcal mol^{-1} with or without hydrogen bonding, respectively, and with a low barrier of 3.60 kcal mol^{-1}. Thus, it is to be expected that this reaction is also readily reversible.

In addition to methanol, water is a constituent of the mixture under catalytic conditions, and thus its addition to **2** in THF was investigated. Interestingly, the intense yellow color of **2** still remained after the addition of 1 equiv of water, but completely faded after 2 equiv. A monohydride species was detected (^{1}H NMR (THF-d_8): δ = −16.5 (t, $^2J_{HP}$ = 18.4 Hz); ^{31}P{^{1}H} NMR (THF-d_8): δ = 76.9 (s)), which is consistent with the formation of Ru−hydroxide **5**, Scheme 7 (see SI 5.1).[28] The coupling constants indicate cis orientation of the hydride to both P donors and a downfield broad peak (^{1}H NMR: δ = 2.9) composed of the resonances of NH and Ru—OH protons. When D_2O was employed under otherwise identical conditions, the intensity of this broad peak dropped significantly, while the hydride signal (and the signals assigned to the ligand backbone protons) remained unchanged. The chemical shift for Ru—H in **5** gradually increased as more water was added, up to a maximum of 4 equiv. This spectroscopic evidence suggests a rapid exchange between **5** and Ru−amido **2** that is faster than the NMR time-scale. This is also consistent with the persistence of the characteristic yellow color of **2** even after the addition of an equivalent of water.

Like Ru—OMe **4** (vide supra), Ru−hydroxide **5** reacted with CO_2 via facile insertion into the Ru—O bond to give a Ru−bicarbonate complex with a strongly downfield shifted N—H due to hydrogen bonding with the carbonate (^{1}H NMR, THF-d_8, δ = 8.25 (bt, J = 10.7 Hz)) (see SI 5.2).[37] **5** also readily reverted back to **2** upon solvent removal. This reversibility, of which similar examples have been reported elsewhere,[38] was supported by theory, Scheme 7. The barrier (2.65 kcal mol^{-1}) was found to be lower than with methanol and less endergonic (0.25 kcal mol^{-1}), which is broadly in agreement with the findings of Lei and co-workers.[19b] However, our results differ from those of Yang[19a] who reported an exergonic reaction (−4.9 kcal mol^{-1}) with a higher barrier (4.8 kcal mol^{-1}), which, with a back-reaction barrier of 9.7 kcal mol^{-1}, does not support the experimental observations.

Under the catalytic conditions, formation of complex **5** is assumed to be an unproductive, off-cycle, intermediate, as there is no reasonable mechanism from which a Ru−dihydride species can be generated. Thus, despite water being necessary to establish full dehydrogenation, it is unsurprising that lower reaction rates are observed when higher proportions of water are present.[9] In addition to solubility issues, this rationale provides a reasonable justification for the use of only low amounts of water in the reaction mixture (9:1 MeOH:water) under optimal conditions.

During catalysis potassium formate is detected in solution,[9] and thus we considered the formation of Ru−formate **6** (see SI 6.1). Metal−formate complexes have been shown to be key intermediates, both in formic acid dehydrogenation[39a] and in CO_2 hydrogenation to formic acid.[39b,c] A number of catalysts bearing noninnocent pincer ligands have afforded highly active systems for these two transformations,[21b,22b,40] and the crystal structures of the involved metal-formate complexes have been reported.[21b,40b,c,e,f] The reaction of **2** with formic acid [**2** + HCOOH = **6**], Scheme 7, was calculated to be more facile than

DOI: 10.1021/jacs.6b05692
J. Am. Chem. Soc. 2016, 138, 14890−14904

with water or methanol. The intermediate and transition state could not be located as the reaction is barrier-less and exergonic by 19.71 kcal mol^{-1}. Indeed, reaction of formic acid with either **2** or **3** yielded a white powder that corresponded to **6**, Scheme 8 (see SI 6.1). Unlike with the addition of MeOH to **2**, which

Scheme 8. Synthesis of 6 by Reaction of Either 2 or 3 with Formic Acid (P = P*i*-Pr$_2$)

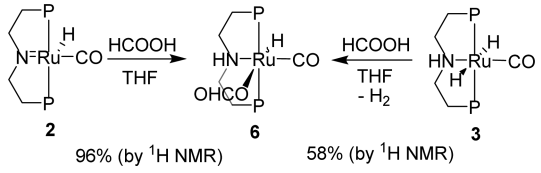

formed a mixture of **4** and **3**, formic acid addition to **2** exclusively gave Ru−monohydride **6**, without signs of Ru−dihydride **3**. NMR data for **6** showed characteristic peaks for formate and hydride ligands (^{1}H NMR (THF-d_8): δ = 8.35 and −18.14) and confirmed their relative geometry about Ru. The NH peak of the backbone resonates at a lower field than in **3** (^{1}H NMR (THF-d_8): δ = 8.61 vs 3.7), indicative of its involvement in intramolecular hydrogen bonding. X-ray analysis of crystals obtained by slow evaporation from a diethyl ether solution, showed the NH and the formate group to be properly oriented for such an interaction, Figure 8. The H1—

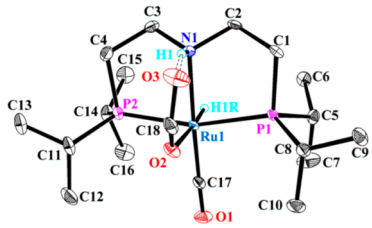

Figure 8. ORTEP view of *anti*-**6** with thermal ellipsoids drawn at the 30% probability level. H atoms other than H1 and H1R have been omitted for clarity.

O3 distance of 1.96(6) Å, the N1—O3 distance of 2.793(4) and the N1—H1—O3 angle of 163(4)° are all characteristic of H-bonding in the complex[41] and share similarities to the related −PPh$_2$ complex (H1—O3 = 2.04(3) Å, N1—O3 = 2.831(3) Å and N1—H1—O3 = 157(3)°),[21b] where such an interaction was also suggested. This intramolecular stabilization will also account for the fact that only one NH isomer is observed spectroscopically in solution. **6** was found to be thermally stable, at least up to 90 °C for 2 h in dioxane, but when treated with 1 equiv of *t*-BuOK in THF-d_8, it reverted back to **2** along with small quantities of **3** (5%) (see SI 6.2). Interestingly, formation of **6** was also possible by reacting complex **3** with CO_2, which we calculated to be exergonic by 6.72 kcal mol^{-1}.

Reactions of Complex 3. We anticipated that Ru−dihydride **3** should be the precursor for a Ru−dihydrogen complex, from which H_2 release is very rapid. Crystals of **3** were obtained from a reaction solution (KOH 8 M; MeOH:H_2O (9:1)). In this complex, the PNP pincer ligand is coordinated in a meridional fashion, with two hydrides trans to each other and cis to the two P donors, and CO sitting trans to nitrogen, Figure 9.

H_2 may be released from **3**, (via Ru−dihydrogen complex), through a four-membered transition-state that yields Ru−

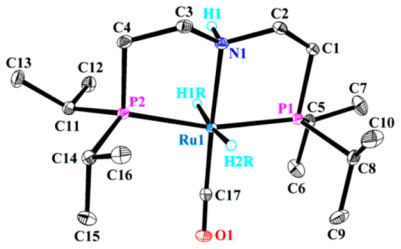

Figure 9. ORTEP view of **3** with thermal ellipsoids drawn at the 30% probability level. Hydrogen atoms other than H1, H1R, and H2R are omitted for clarity.

amido **2**. A concerted H_2 addition onto **2** was calculated to be exergonic by 2.31 kcal mol^{-1} with a barrier of 18.76 kcal mol^{-1}, Scheme 7. This is consistent with experimental observations under aprotic conditions, as **3** was found to be relatively stable and dehydrogenation could only be partially promoted by thermal treatment: heating **3** (62 mM) in dioxane-d_8 to 100 °C for 50 min in a sealed NMR tube furnished only 20% of the dehydrogenated Ru−amido complex **2**, in parallel with H_2 evolution. H_2 was then shown to add back onto **2** to form **3** within a few hours (see SI 7.1). The observed low conversion, as well as the slow back reaction are consistent with theory, which reveals that the reaction is slightly endergonic and can form an equilibrium under an H_2 atmosphere in favor of **3**. Yang[19a] and Lei and co-workers[19b] calculated highly exergonic reactions (11.9 and 7.6 kcal/mol, respectively), which do not support reversibility between **2** and **3** under a H_2 atmosphere.

A solvent-mediated process may facilitate H_2 release from complex **3**,[19a] where MeOH (or H_2O) shuttles a proton from nitrogen to the hydride, presumably proceeding through intermediates **I** and **II**, Scheme 9.[42] The barrier for the solvent

Scheme 9. Hydrogen Generation via Protonation of 3 (P = P*i*-Pr$_2$)

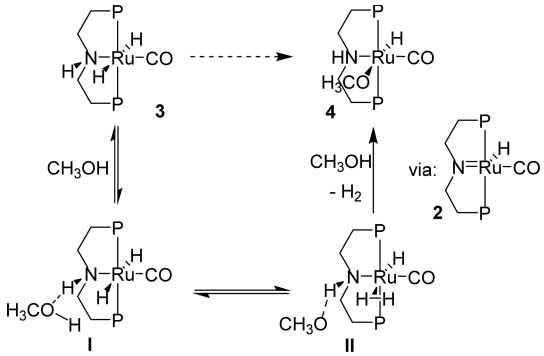

assisted H_2 loss from **3** was then considered: the direct addition of H_2 to **2** reduced to 13.71 kcal mol^{-1} with MeOH assistance compared to 18.76 without. After the addition of 1 equiv of MeOH to a solution of **3** in THF-d_8 **4** appeared, and the release of H_2 gas was observed (see SI 7.2). However, despite the relative amount of **4** increasing with further equivalents of added methanol, incomplete conversion (78%) was observed, even with 50 equiv. As indicated above, this reaction [**3** + CH_3OH = **4** + H_2] is endergonic by 3.19 kcal mol^{-1}, thermodynamically unfavorable, and thus a large excess of methanol is necessary to fully convert **3** to **4**.

Both the hydricity[43] of the Ru—H and the acidity of the proton source are important when the rate of H_2 release from **3**

DOI: 10.1021/jacs.6b05692
J. Am. Chem. Soc. 2016, 138, 14890−14904

is considered. Consistently, by employing the more acidic formic acid, quantitative formation of Ru−formate **6** was observed with concomitant evolution of H_2 gas. In agreement, this thermodynamically favorable reaction [**3** + HCOOH = **6** + H_2] was calculated to be exergonic by 14.70 kcal mol^{-1}. In addition, the cationic monohydride PNP $Ru^+BF_4^-$ complex was rapidly prepared by reaction of **3** with 1 equiv of HBF_4 and release of H_2 gas (see SI 7.3).

The difference between the ^{1}H and ^{31}P NMR chemical shifts of complex **3** (in THF-d_8) and those observed under the reaction conditions (MeOH:H_2O (9:1), 8 M KOH, 91 °C) is within the reasonable range expected from such a dramatic change in solvent environment. However, the multiplicity of the hydride peak is very different and the triplet observed in basic MeOH:H_2O (9:1) (see SI 8.2) is inconsistent with the multiplet observed in THF-d_8.[44] To investigate this, methanol was sequentially added to **3** in THF-d_8, which instigated peak broadening of one of the super imposed Ru−hydride signals in the multiplet, leading to the triplet observed under catalytic conditions (see SI 7.2). We interpret this as additional evidence for the interaction of methanol and **3** through hydrogen-bonding, Scheme 9. The NMR signals were also progressively shifted to higher fields, which is further indication of dihydrogen bonding.[45] A comparable effect was reported by Schneider and co-workers.[46]

Studies under catalytic conditions. As many high performing catalysts contain PNP ligands with aliphatic backbones,[3] we investigated the possible involvement of Ru−enamido complex **2-E** in a mechanism proposed using a related complex,[30,47] Scheme 10 (see SI 8.1). No incorporation of

Scheme 10. Possible Metal-Ligand Bifunctional Catalysis through Ligand Backbone Deprotonation (P = P*i*-Pr$_2$)

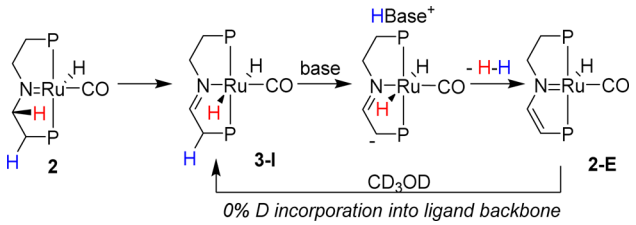

deuterium into the ethylene bridges of the backbone was detected (^{1}H NMR) under the reaction conditions, as would be expected from such a pathway in deuterated solvents. In addition, the isomerization between **2** and **3-I** was calculated to be endergonic by 8.83 kcal mol^{-1}. Thus, we conclude this pathway to be unfeasible.

Stoichiometric reactions of the Ru−amido complex **2** demonstrated that methanol, water, and formic acid can readily add across the Ru—N bond, affording the corresponding 18-electron monohydride species **4**, **5**, and **6**, respectively. The more acidic the protic compound, the more stable the monohydride adduct was formed. Addition of base to **6** under aprotic conditions reversed this reaction back to **2**. However, under the basic catalytic dehydrogenation conditions (MeOH:H_2O (9:1), KOH 8 M) it was never possible to either observe the characteristic yellow color of **2** or spectroscopically detect this complex. Two other species were detected under these conditions, albeit using an increased concentration of catalyst **1a** (20 mM) and at room temperature (see SI 8.2). The first was thought to be the Ru−monohydride methoxy species **4** (^{1}H NMR δ = −18.17; ^{31}P NMR: δ = 74.05) and the second possibly the Ru−dihydride **3** (^{1}H NMR: δ = −7.20; ^{31}P NMR: δ = 88.64). Due to the nontrivial task of characterizing rapidly equilibrating species under the reaction conditions, where hydrogen bonding adds further complication, it was not possible to unambiguously identify the monohydride species by spectroscopic means.

NMR spectra showed that the ratio of **3** and **4** was unchanged from room temperature to 90 °C. With continued heating, free formate was detected, alongside monohydride Ru−formate **6** (^{13}P NMR: δ = 74.64) (see SI 8.2). A precipitate was also generated after prolonged heating (60 min), which was isolated, analyzed (^{13}C NMR), and found to contain a mixture of HCOOK and K_2CO_3/$KHCO_3$,[48] i.e., products of partial and full methanol dehydrogenation, respectively.

Despite efficient hydrogen release from preformed **3** under acidic conditions, vide supra, catalysis is most efficient under highly basic conditions, implying a high pH is necessary to turnover the catalytic cycle. To test for the influence of KOH on the ratio of catalyst resting states, its concentration was incrementally increased under catalytic conditions, and the proportion of dihydride to monohydride was recorded by ^{1}H NMR (see SI 8.3). **3** only appeared after 3.4 M KOH had been added. Raising the concentration beyond 3.4 M further increased the proportion of **3** to **4** by reducing its propensity for protonation. When a strong base was added (2 equiv *t*BuOK) to a solution of **4** under aprotic conditions, full conversion to **3** was observed, vide supra.

The complexity observed in the hydride multiplet of **3** in THF-d_8, could also be removed through the addition of strong base. When BuLi was added to **3**, the amine in the pincer ligand was deprotonated to give the trans Ru−dihydride amidate complex (**3**$^-$) (see SI 8.4). Disappearance of the backbone NH peak was accompanied by simplification of the hydride multiplet that was slightly shifted upfield; all features consistent with formation of **3**$^-$. Protonation of **3**$^-$ with water directly led back to **3**. On the basis of kinetic studies, Ru−amidate complexes have been postulated in ketone hydrogenations using Noyori-type catalysts.[49] The increased hydride nucleophilicity in the corresponding anionic catalysts, which were detected at low temperature, promotes hydrogenation of the less reactive amides and imides.[50] Thus, the evidence presented here suggests the high pH of the catalytic conditions will initiate backbone NH deprotonation. This is consistent with the slight discrepancy observed in the chemical shifts between the reaction conditions and the protonated material. By DFT, we calculated the energetics of NH backbone deprotonation in the resting states and found the deprotonation to be barrier-less and extremely exergonic, Scheme 11. The pK_a of the backbone N—H in **4** and **3** was calculated (PBE0-NL/def2-TZVPP) to be 9.09 and 8.24, respectively.[51] With a steady-state pH between 10 and 13, this clearly indicates that the catalyst is largely deprotonated.

Observations from these in situ experiments thus suggest the existence of two potential wells in the multistep process, with deprotonated monohydrides **4**$^-$, **5**$^-$ or **6**$^-$ and dihydride **3**$^-$ as catalytic resting states. Only Ru−formate complex **6** was recovered from the reaction mixture, which reconfirmed its relative stability to **4**. When the dehydrogenation of aqueous methanol was carried out using $^{13}CH_3OH$, ^{13}C-**6** was isolated, where the ^{13}C label was only incorporated into the formate group and was not detected in the coordinated CO (see SI 8.5).

Mechanistic Proposal for Complex 1a. Crucial for this dehydrogenation process are the C—H cleavage and the

DOI: 10.1021/jacs.6b05692
J. Am. Chem. Soc. 2016, 138, 14890−14904

Scheme 11. DFT Calculated Energy (kcal mol^{-1}) of Anionic Complex Formation (P = P*i*-Pr$_2$)

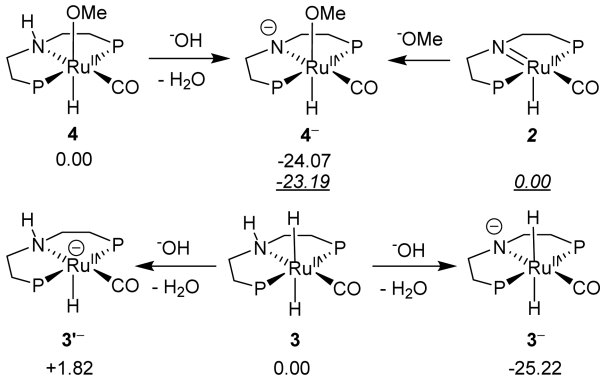

transfer of hydride from methanol, gemdiol, or formate to the Ru center. Several scenarios can be envisaged for these elementary steps (shown for methanol in Scheme 12). Previously, we had proposed a direct outer-sphere addition of methanol onto **2**, Scheme 3 and Scheme 12 (path A).[9,19] On the basis of our current findings, we now believe that this pathway is unlikely to occur: not only have we shown that **4** is rapidly formed from **2** in the presence of MeOH, but also that the addition of formic acid to **2** exclusively gives Ru−formate complex **6** without sign of dihydride **3** formation. Moreover, it was not possible to computationally locate a transition state for the direct process **A** and there is also no reasonable rationale for the dependency of the rate on the base concentration.

Taking into account the intermediacy of **4**, an alternative pathway **B** could involve a nontraditional β-hydride elimination pathway. However, not only were we unable to locate a transition state, it is unprecedented for this type of complex and again does not explain the role of base. Hence, we considered pathways that are more likely to occur in the high pH environment necessary for optimal catalytic activity. Deprotonation of **4** may occur at the methoxide —C—H (pathway **C**) or the backbone N—H. Pathway **C** leads directly to anionic complex **8**, as no intermediate could be located due to rapid formaldehyde dissociation. However, backbone N—H deprotonation leading to **4**$^-$ was found to be much more exergonic than C—H deprotonation (−23.19 vs 13.23 kcal mol^{-1}), thus disfavoring pathway **C**. The high concentration of KOH (pH > 10) also means there will be a substantial proportion of methoxide present that directly forms **4**$^-$ from **2**. **4**$^-$ may initiate C—H cleavage of the bound methoxide with ensuing formaldehyde loss (pathway **D**). However, this reaction (**4**$^-$ = **8** + CH_2O) is highly endergonic (33.45 kcal mol^{-1}) and no transition state for the β-hydride-type elimination could be located. Moreover, the proton shift from nitrogen to Ru that generates resting state **3**$^-$ from **8** would require overcoming a barrier of 6.67 kcal mol^{-1}.

Additional efforts to locate a more viable reaction pathway focused on the frontier orbital interaction between **2** and

Scheme 12. Possible Pathways for the Key Step Involving C—H Bond Cleavage and Ru−Dihydride Formation (P = P*i*-Pr$_2$)[a]

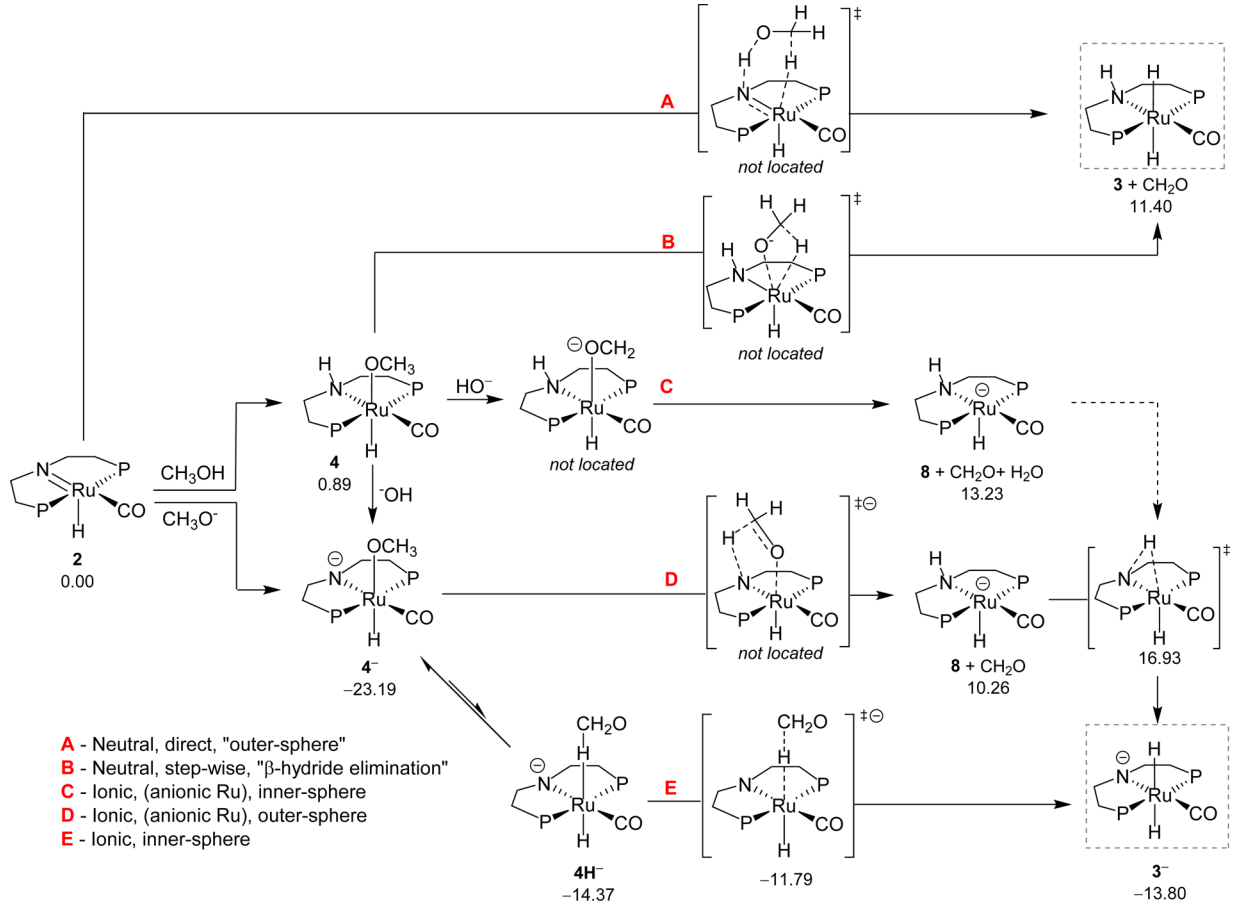

[a]Energies are given in kcal mol^{-1}.

DOI: 10.1021/jacs.6b05692
J. Am. Chem. Soc. 2016, 138, 14890−14904

Scheme 13. DFT Calculated Energies (kcal mol^{-1}) for Pathway E (P = P*i*-Pr$_2$)

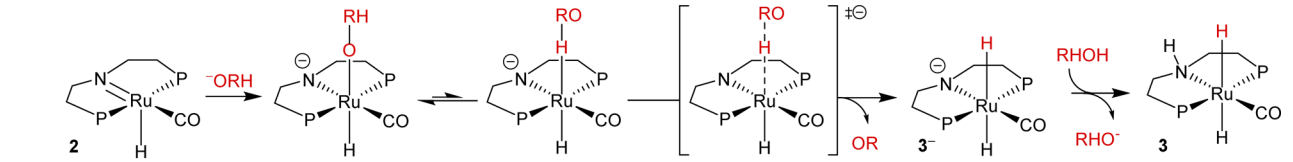

R: CH_2	0.00	-23.19	**4**$^-$	-14.37	**4H**$^-$	-11.79	TS(**4H**$^-$/**3**$^-$)	-13.80		11.41
R: CHOH	0.00	-6.04	**7**$^-$	-9.51	**7H**$^-$	-8.93	TS(**7H**$^-$/**3**$^-$)	-18.18		-9.15
R: CO	0.00	-7.15	**6**$^-$	-4.90	**6H**$^-$	8.19	TS(**6H**$^-$/**3**$^-$)	0.98		-12.99

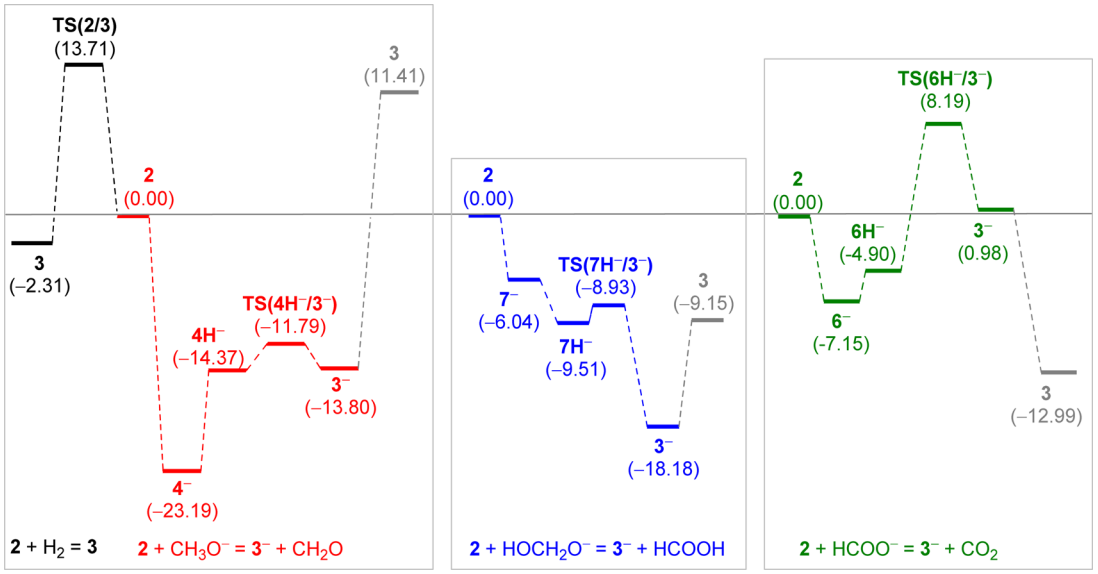

Figure 10. Potential energy surface for the key step in pathway E involving C—H bond cleavage and Ru–dihydride formation. Energies are given in kcal mol^{-1}. Protonations of **3**$^-$ to **3** in each step are with CH_3OH, $HOCH_2OH$, and HCOOH, respectively.

methoxide, gem-diolate, and formate (see SI 14). This analysis demonstrates that both the negatively charged O atom and the H—C atom can coordinate to the Ru center of complex **2** (pathway **E**), similar to that proposed with Fe,[12b,40i] and Ir,[20] and that the two isomers exist in a dynamic equilibrium. The O-coordination of methoxide to **2** generating **4**$^-$ was found to be exergonic by 23.19 kcal mol^{-1}, whereas the H-coordinated isomer **4H**$^-$ is less stable by 8.82 kcal mol^{-1}, Scheme 13. The barrier for C—H cleavage and formation of Ru–dihydride **3**$^-$ and formaldehyde is only 2.58 kcal mol^{-1} with an overall effective barrier of 11.40 kcal mol^{-1}. In attempts to locate lower energy pathways, we considered cyclic transition states with bridging solvent molecules for pathways **A**, **B**, **D**, and **E**. However, we were unable to locate such structures. Nevertheless, pathway **E** represents an energetically viable pathway that is consistent with the experimental results.

The formation of **7**$^-$, by O-coordination of gem-diolate to **2**, was found to be exergonic by 6.04 kcal mol^{-1}, with the H-coordinated isomer **7H**$^-$ *more* stable by 3.47 kcal mol^{-1}, Scheme 13. The barrier for the C—H bond dissociation leading to formic acid and **3**$^-$ is only 0.58 kcal mol^{-1}. When considering a hydrogen bonding interaction between the OH group and the ligand backbone N atom for **7H**$^-$, this step becomes barrierless; directly forming formate and **3** in a highly exergonic (26.11 kcal mol^{-1}) reaction [**2**+$^-$OCH$_2$OH = **3** + HCO$_2^-$]. The fact that **7H**$^-$ is predicted to be more stable than **7**$^-$, combined with low activation barriers for its further reaction, suggests this step should be rapid and highly favorable. This is in-line with experimental observations, as the gem-diolate (or CH_2O) has never been detected spectroscopically in situ, nor has any complex containing it, i.e., **7**$^-$ or **7H**$^-$. Formaldehyde was indeed tested for (Merck MColortest) under the reaction conditions and returned a negative result (see SI 9.1), while a reaction solution containing added formaldehyde returned a positive test (>1.5 mg/L). The possibility of rapid, uncatalyzed, base-induced formaldehyde decomposition[52] was considered as a possible rationale for the negative result. However, negligible volumes of gas were formed when formaldehyde was added to a standard reaction in the absence of precursor **1a** (see SI 9.2). Thus, we are confident the DFT calculations are correct in modeling this catalytic step to be very rapid indeed.

For the O-coordination of formate to **2** leading to **6**$^-$, the reaction is exergonic by 7.15 kcal mol^{-1}, with the H-coordinated isomer **6H**$^-$ less stable by 2.25 kcal mol^{-1}. The barrier for the C—H bond dissociation leading to CO_2 and **3**$^-$ is 13.09 kcal mol^{-1}, with an overall effective barrier of 15.34 kcal mol^{-1}. The potential energy surface shown in Figure 10 implies that there should be two main resting states, **4**$^-$ and **3**$^-$, which are detected spectroscopically, vide supra. **6**$^-$ was also observed (^{1}H and ^{31}P NMR) throughout the reaction. As **6**$^-$ faces a C—H cleavage barrier of 15.34 kcal mol^{-1}, it is a reasonable species to detect in situ.

Our computed barrier for the direct and methanol promoted reaction of **2** + H_2 = **3** is 18.76 and 13.71 kcal mol^{-1}, respectively, and is exergonic by 2.31 kcal mol^{-1}. While Yang calculated the corresponding barrier as 29.5 and 21.8 kcal mol^{-1}, respectively, with an endergonic reaction of 11.9 kcal mol^{-1}, Lei and co-workers showed the barrier to be 27.1 and

DOI: 10.1021/jacs.6b05692
J. Am. Chem. Soc. 2016, 138, 14890–14904

21.0 kcal mol^{-1}, respectively and endergonic by 7.6 kcal mol^{-1}.[19] Our experimental observations, such as the reversibility between **3** and **2** under H_2 atmosphere and the facile formation of **3** from **2**, support the computed exergonic property of the reaction. For the first dehydrogenation step that leads to formaldehyde, the obtained effective barriers are largely in agreement with those of Yang and Lei and co-workers. However, for the dehydrogenation of hydroxymethanolate, higher barriers were calculated from Yang and Lei and co-workers that do not agree with our experimental and theoretical results (0.58 vs 14.3 and 5.2 kcal mol^{-1}, respectively). For the last dehydrogenation step, we found an effective barrier of 13.54 kcal mol^{-1}, while Lei and co-workers reported one of about 31 kcal mol^{-1}, and Yang of 23.4 kcal mol^{-1}. Yang found the O-coordinated formate (**6**$^-$) to be more stable than the H-coordinated (**6H**$^-$) by 7.9 kcal mol^{-1}, which is larger than our value of 2.25 kcal mol^{-1}. The closer agreement between the experimental results and calculations provides confidence in our computational models and methods.

On the basis of the experimental and theoretical findings, a catalytic cycle for methanol dehydrogenation can now be proposed, Scheme 14, that includes a justification for the highly basic conditions. Specifically, we can summarize three major roles for KOH:

- First, it is required to dehydrochlorinate the precatalyst **1a**
- Second, formation of the key H-coordinated intermediates (**4H**$^-$, **7H**$^-$ and **6H**$^-$) is found to readily occur from deprotonated O-coordinated intermediates **4**$^-$, **7**$^-$ and **6**$^-$
- Lastly, the key dehydrogenation step that produces Ru–dihydride (**3**$^-$) species from the monohydride species (**4**$^-$, **7**$^-$ and **6**$^-$) is promoted by base. By sequestration of formaldehyde, formic acid, and CO_2 byproducts the high base concentration renders these steps thermodynamically feasible and drives the reaction forward.

Scheme 14. Proposed Catalytic Cycle for Aqueous Methanol Reforming (P = *i*-Pr$_2$)

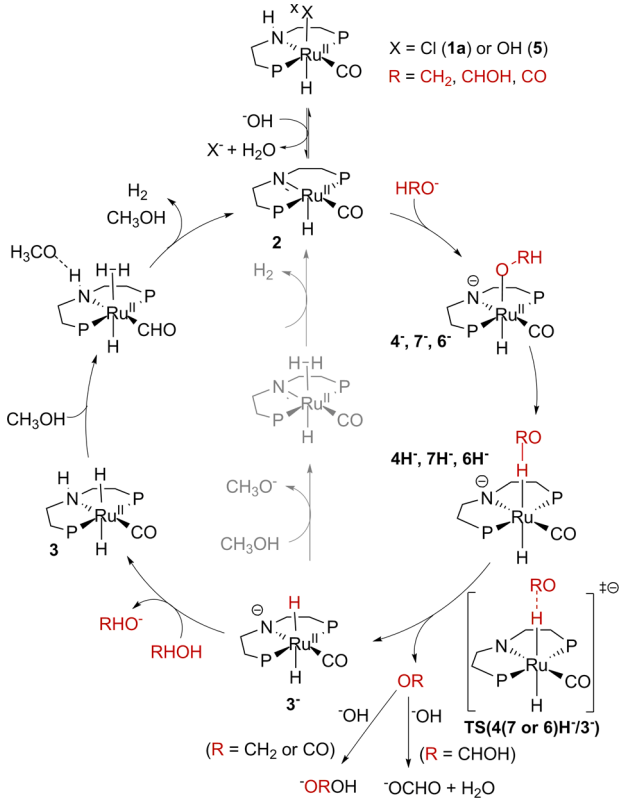

Following the formation of **3**$^-$, we propose protonation at nitrogen to occur, followed by a MeOH-assisted H_2 elimination. Depending on the nature of the acid, direct protonation may also be a possibility (grey pathway, Scheme 14). Interestingly, the inner-sphere C—H cleavage step does not involve ligand participation any more than acting as a strongly donating anionic ligand, a finding that might be critical in the development of new active catalyst systems.

Mechanistic Proposal with Ru–Complex Me-1a. As shown in Scheme 14, N-deprotonated complexes **4**$^-$, **6**$^-$, and **7**$^-$ are key intermediates in the catalytic cycle. We also demonstrated that **Me-1a** is a proficient catalyst for aqueous basic MeOH dehydrogenation, vide supra. Although its catalytic activity is significantly lower, **Me-1a** can catalyze all three MeOH dehydrogenation steps, as both formate and carbonate were detected after allowing the reaction to reach high conversion. Obviously, these observations cannot be rationalized on the basis of our proposed mechanism. Thus, stoichiometric studies and theoretical calculations were performed using **Me-1a**.

In a typical catalytic experiment under the standard reaction conditions (MeOH:H_2O (9:1), KOH 8M) only one species was observed (^{1}H NMR: δ = −6.2 (t, $^2J_{HP}$ = 17.4 Hz), −6.7 (t, $^2J_{HP}$ = 20.8 Hz); ^{31}P{^{1}H} NMR: δ = 87.5 (s)) that we suspected was Ru–dihydride **Me-3** (see SI 10.1). To confirm the identity of this species, **Me-3** was independently prepared, Scheme 15 (see SI 10.2).[21d] The compound was obtained as a mixture of two isomers in a 98:2 ratio, which, based on NMR data, were identified as *trans*-**Me-3** (^{1}H NMR (toluene-d$_8$): δ = −6.02 (tm, $^3J_{HP}$ = 20.0 Hz), −5.75 (tm, $^3J_{HP}$ = 18.5 Hz); ^{31}P{^{1}H} NMR (toluene-d$_8$): δ = 89.59 (s)) and one of the two possible cis isomers, *cis*-**Me-3** and *cis*-**Me-3′** (^{1}H NMR (toluene-d$_8$): δ = −15.77 (td, J_{HP} = 18.6 Hz, J_{HH} = 5.2 Hz), −7.13 (td, J_{HP} = 21.7 Hz, J_{HH} = 5.2 Hz); ^{31}P{^{1}H} NMR (toluene-d$_8$): δ = 86.78 (s)) that depend on the relative orientation of methyl and hydride (′ = cis). The spectroscopic data indicate the presence of 2 equiv phosphorus donors cis orientated to the hydrides. The hydrides in *trans*-**Me-3** have very close chemical shifts, whereas the two hydrides in the cis isomers are very different, due to the differing trans influence being exerted. The NMR data recorded under the reaction conditions are most similar to that of *trans*-**Me-3**, and thus we propose this to be the resting state of the catalytic cycle.

Scheme 15. Preparation of *trans*- and *cis*-Me-3 (P = P*i*-Pr$_2$)

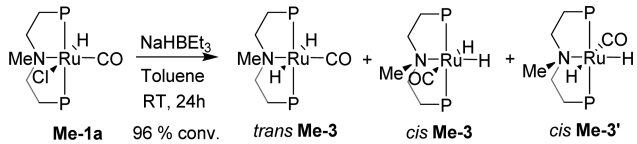

Protonation of **Me-3** by alcohol is an important step in the catalytic cycle.[53] An excess (2.8 equiv) of CH_3OD was added to a sample of **Me-3** in C_6D_6 (see SI 10.3). Two new species were formed whose spectroscopic data are consistent with monodeuterated *trans*-[^{2}**H**]-**Me-3** (^{1}H NMR (C_6D_6): δ = −5.64 (t, $^3J_{HP}$ = 18.1 Hz)) and *trans*-[^{2}**H**]-**Me-3′** (^{1}H NMR (C_6D_6): δ = −5.96 (t, $^3J_{HP}$ = 20.0 Hz)) that arise from H/D

DOI: 10.1021/jacs.6b05692
J. Am. Chem. Soc. 2016, 138, 14890–14904

exchange between **Me-3** and CH_3OD, Scheme 16. Depending on the relative orientation of NMe and D, the two

Scheme 16. Hydridic H/D Exchange in Me-3 upon Reaction with CH_3OD (P = P*i*-Pr_2)

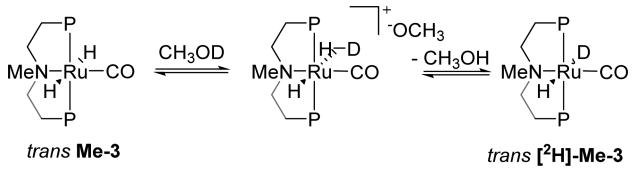

monodeuterated isomers were formed in equimolar amounts, indicating that the rates of exchange are equal no matter the orientation of NMe. This is in contrast to unmethylated **3**, where, through hydrogen bonding, N—H orientation was found to be highly influential on the process.[46] Coordinatively saturated 18e$^-$ **Me-3** must protonate to form a transient and undetected Ru−dihydrogen complex. Indeed, in the presence of added methanol the hydride signals of *trans*-**Me-3** are both shifted upfield (^{1}H NMR: $\Delta\delta$ = ca. −0.10, ^{31}P NMR: $\Delta\delta$ = ca. −0.25) (see SI 10.4). Such changes are typical of dihydrogen bond formation and result from the fast equilibrium between the dihydrogen-bonded complex and free *trans*-**Me-3**.[45]

As MeOH is only a weak acid, a large excess of alcohol is necessary to shift the equilibrium toward protonation of the metal hydride and to eliminate H_2.[53] Attempts to displace the equilibrium toward H_2 elimination by heating to 90 °C were not effective. Along with the observed H/D exchange process, vide supra, two new species were observed when increasing quantities of MeOH were added to **Me-3** in toluene-d_8. We propose these undefined species to be either *trans*-**Me-3** hydrogen bonded to MeOH or a cationic Ru−dihydrogen complex. However, even with 50 equiv of MeOH, no H_2 was observed to evolve (see SI 10.4). Indeed, theory predicts that protonation of Ru−dihydride **Me-3** by MeOH to afford the corresponding ruthenium methoxide **Me-4** (or **Me-4′**) is endergonic by 8.02 (or 6.94 kcal mol^{-1}), Figure 11.

The key dehydrogenation step is the reformation of **Me-3** from **Me-4**. One possibility would be to proceed via β-hydride elimination, where the coordinatively saturated 18-e$^-$ species requires temporary decoordination at a cis site.[54−56] However, this seems highly unlikely considering the stability of the pincer and CO ligands. Indeed, no evidence for this could be gained from NMR. A dissociative β-hydride abstraction is able to circumvent this problem. It should be accelerated in a polar medium by promoting alkoxide dissociation,[20,27d,57] however, DFT was not able to find a suitable low energy pathway and this would not fully explain the experimental data.

Under neutral conditions, a similar mechanism for **4** to **3** in the unmethylated catalyst, via H-coordination of substrate to the Ru-center, provided a viable route for C—H cleavage and hydride delivery, Figure 11. The overall dehydrogenation of methanol into formaldehyde and H_2 is calculated to be endergonic by 13.72 kcal mol^{-1} and the corresponding effective barrier is 22.40 kcal mol^{-1}. In contrast, the dehydrogenation of methandiol (to HCOOH and H_2) and formic acid (to CO_2 and H_2) are predicted to be exergonic processes by −6.84 and −10.68 kcal mol^{-1}, respectively, Figure 11. Protonation of **Me-3** by methanediol resulting in the formation of **Me-7** or **Me-7′** is, however, endergonic by 5.52 or 4.22 kcal mol^{-1}, respectively. The effective barrier for this second step is calculated to be 13.62 kcal mol^{-1}, although the H-coordinated ruthenium methoxide species **Me-7H** could not be located. Protonation of **Me-3** by formic acid to **Me-6** and **Me-6′** was calculated to be exergonic by 7.77 and 8.63 kcal mol^{-1}, respectively, Figure 11. The observation that 1 equiv of formic acid is sufficient to promote H_2 liberation and quantitative conversion of **Me-3** to **Me-6** is in-line with this theory. **Me-6** was prepared as a mixture of two isomers (major: 81%, ^{1}H NMR (toluene-d_8): δ = −17.26 (t, J_{HP} = 19.4 Hz); ^{31}P{^{1}H} NMR (toluene-d_8): δ = 70.56 (s); minor: 19%, ^{1}H NMR (toluene-d_8): δ = −17.16 (t, J_{HP} = 18.7 Hz); ^{31}P{^{1}H} δ = 72.95 (s)) depending on the relative orientation of NMe and formate (see SI 10.5). Indeed, the calculated free energy difference of 0.86 kcal mol^{-1} corresponds to a ratio of 81 to 19 in favor of **Me-6′**, in perfect agreement with experiment. Heating **Me-6** for 3 h at 90 °C triggered partial (42%) conversion to **Me-3** (cis−19% and trans−81%) and gas evolution, experimentally validating the lower barrier (about 8 kcal mol^{-1}) found for this process (see

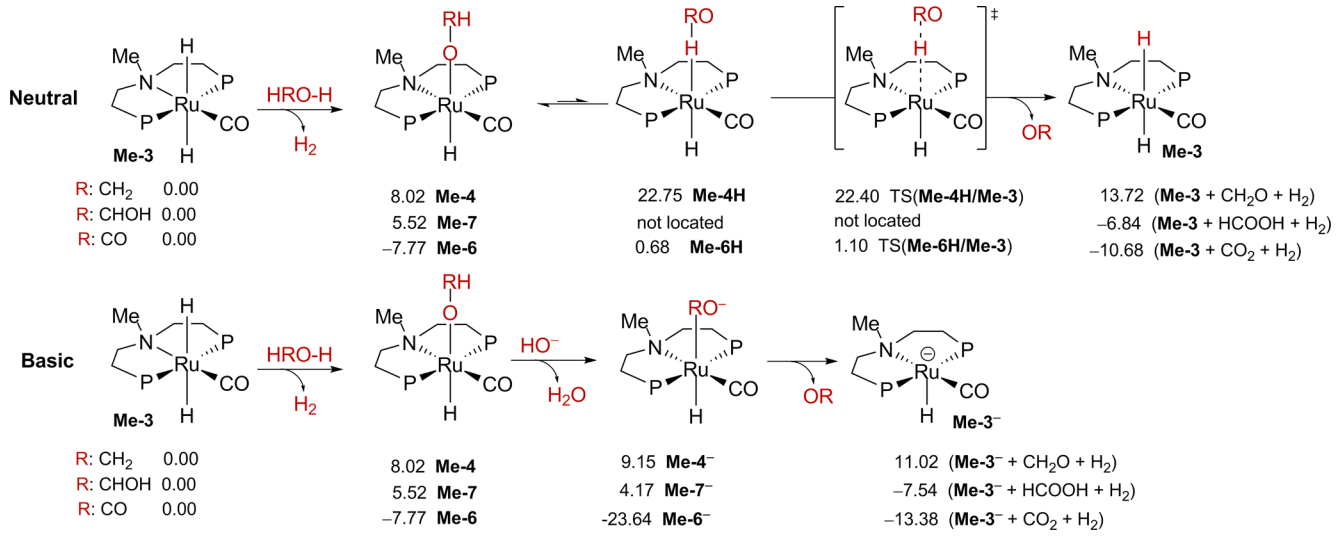

Figure 11. Potential energies (kcal mol^{-1}) for the key C—H bond cleavage step and Ru−dihydride formation under neutral and basic conditions. Only showing energies for the trans hydride/methyl monohydride isomer (*P* = *i*-Pr_2).

DOI: 10.1021/jacs.6b05692
J. Am. Chem. Soc. 2016, 138, 14890−14904

SI 10.6). Our calculations suggest that methanol dehydrogenation to formaldehyde is the least facile of the three steps when catalyzed by **Me-1a** precatalyst. This is in contrast to the process promoted by **1a**, in which formic acid dehydrogenation is the least facile step.

The base is clearly necessary to promote the dehydrogenation with **Me-1a**, as no reaction is observed in its absence, Figure 5. As well as sequestering the formaldehyde, formic acid and CO_2 byproducts and providing a thermodynamic driving force, KOH is likely to be involved in the key-step. Indeed, **Me-3** was readily generated from **Me-1a** after treatment with KOMe in toluene (see SI 10.7). In addition, the reaction of cationic **Me-1-BAr$^F_4$** (obtained from the reaction of **Me-1a** with Na[BAr$^F_4$] (Ar^F = 3,5-$C_6H_3(CF_3)_2$) (^{1}H NMR (THF-d_8): δ = −21.6 (bs); ^{31}P{^{1}H} NMR (THF-d_8): δ = 67.1 (bs)) with 5 equiv of MeOH in THF-d_8 only afforded a weakly coordinated cationic adduct (^{1}H NMR (THF-d_8): δ = −20.5 (bs); ^{31}P{^{1}H} NMR (THF-d_8): δ = 68.1 (bs)) that does not undergo any C—H cleavage or hydride delivery. Only after the addition of KOMe did **Me-3** rapidly form. Thus, **Me-3** is formed more readily in the presence of methoxide and explains the increase in rate observed at lower base concentrations, Figure 5.

To further rationalize these observations, we considered possible promotional roles of base in the key-step and calculated a route more favorable than the neutral pathway, Figure 11. Thus, starting from **Me-4**, deprotonation of the bound —OCH_3 group was shown to result in the formation of **Me-4**$^-$, where the coordination switches from Ru—OCH_2 to Ru—CH_2O. **Me-3**$^-$ is generated following rapid CH_2O dissociation. Ru—OCH_3 (**Me-4**) deprotonation and CH_2O dissociation are endergonic by 1.13 and 1.87 kcal mol^{-1}, respectively. The formed CH_2O can then be consumed by base into hydroxymethanolate. In a similar manner, deprotonation of the C—H bond of the bound —O—CH_2—OH group within **Me-7** shifts the coordination from O- to C-, which results in formation of **Me-7**$^-$ and subsequent dissociation of HCOOH to generate **Me-3**$^-$. Ru—OCH_2—OH deprotonation and HCOOH dissociation is exergonic by 1.35 and 11.71 kcal mol^{-1}, respectively. Starting from **Me-6**, an analogous route was located, wherein deprotonation of the Ru—OCHO group accompanied O- to C-coordination exchange and is exergonic by 15.87 kcal mol^{-1}. Interestingly, CO_2 dissociation was found to be endergonic by 10.26 kcal mol^{-1}, indicating very strong CO_2 coordination.

The activity of **Me-1a** was shown to increase with increasing base concentration up to 4 M KOH, after which it dropped, Figure 5. This "bell-shaped" behavior indicates that base is playing at least two competing roles. **Me-3** was found to be much more stable than **3** toward protonation and was observed after the addition of 200 equiv of KOH (see SI 8.3 and 10.8). This enhanced stability toward protonation is one reason why the rates of methanol dehydrogenation employing **Me-1a** are slower than with **1a**. Thus, at high pH, the reaction is attenuated by the stability of **Me-3** toward protonation and can explain the drop-off in rate that is observed, Figure 5. The stabilization of **3** by high pH is much less than **Me-3**, and consequently the counteracting decrease in rate is much less pronounced.

CONCLUSIONS

We have characterized the reactivity of catalyst **1a** and **Me-1a** in aqueous methanol dehydrogenation and proposed mechanisms based on our spectroscopic, experimental, and theoretical investigations. At constant temperature, rates of reaction increased with increasing KOH concentrations for catalyst **1a**. A range of Ru complexes that are possible catalytic intermediates were independently prepared, isolated, and characterized by spectroscopy and X-ray crystallography, and their reactivity examined under aprotic conditions. Ru—amido **2** was highly reactive with MeOH, formic acid and water and provided mono and dihydride Ru complexes. These hydride complexes were found to be in an apparent equilibrium that could be perturbed by base, to dihydride **3**, or acid, to monohydride **4**. Under catalytic conditions, the resting states were shown to be the N—H deprotonated **3**$^-$ and **4**$^-$ complexes. In addition to experimentally disproving a number of other pathways, DFT rationalized a full mechanistic cycle involving these anionic species in the key step. Thus, it was demonstrated that the ligand does not play a cooperative role in the inner-sphere C—H cleavage step.

Precatalyst **Me-1a** was found to be active, albeit less than **1a**. A number of possible methylated intermediates were prepared, and their reactivity investigated. **Me-3** was found to be more stable than **3** to protonation, which accounts for the lower rates observed under the standard reaction conditions. The rate of dehydrogenation increased with added KOH up to 5 M, but dropped with higher concentrations. KOH is essential to ensure methoxide is present in solution, from which hydride transfer to Ru proceeds to afford dihydride **Me-3**. However, at higher KOH concentrations, the stability of **Me-3** is too high and its protonation rate decreases.

We anticipate these results to be particularly valuable in the development of new catalysts that can operate at lower base concentrations and temperatures in this important reaction.

ASSOCIATED CONTENT

Supporting Information

The Supporting Information is available free of charge on the ACS Publications website at DOI: 10.1021/jacs.6b05692.

Experimental and computational details and characterization data (PDF)
X-ray crystallographic data for **1a** (CIF)
X-ray crystallographic data for **2** (CIF)
X-ray crystallographic data for **3** (CIF)
X-ray crystallographic data for **6** (CIF)
X-ray crystallographic data for **Me-1a** (needle) (CIF)
X-ray crystallographic data for **Me-1a** (block) (CIF)

AUTHOR INFORMATION

Corresponding Author

*matthias.beller@catalysis.de

Author Contributions

$^\perp$E.A. and A.J.J.L. contributed equally.

Notes

The authors declare no competing financial interest.

ACKNOWLEDGMENTS

E.A. would like to thank the DAAD, Programme n. 50015559, for a scholarship. A.J.J.L. would like to thank the Alexander von Humboldt Foundation for generous funding. L.K.V. would like to thank the VCI for a scholarship (n. 196241). M.N. would like to thank the Marie Curie FP7 International Outgoing Fellowship (IOF n. 327565) and the Danish Council for Independent Research (n. 12-131997) for financial support.

DOI: 10.1021/jacs.6b05692
J. Am. Chem. Soc. 2016, 138, 14890−14904

REFERENCES

(1) Armaroli, N.; Balzani, V. *Chem. - Asian J.* **2011**, *6*, 768−784.
(2) Armaroli, N.; Balzani, V. *ChemSusChem* **2011**, *4*, 21−36.
(3) Bagotsky, V. S. *Fuel Cells: Problems and Solutions*, 2nd Ed.; Wiley-VCH: Weinheim, 2012.
(4) (a) Dalebrook, A. F.; Gan, W.; Grasemann, M.; Moret, S.; Laurenczy, G. *Chem. Commun.* **2013**, *49*, 8735−8751. (b) Eberle, U.; Felderhoff, M.; Schüth, F. *Angew. Chem., Int. Ed.* **2009**, *48*, 6608−6630.
(5) (a) Trincado, M.; Banerjee, D.; Grützmacher, H. *Energy Environ. Sci.* **2014**, *7*, 2464−2503. (b) Brethauer, S.; Studer, N. H. *Chimia* **2015**, *69*, 572−581. (c) Goeppert, A.; Czaun, M.; Jones, J.-P.; Prakash, S. G. K.; Olah, G. A. *Chem. Soc. Rev.* **2014**, *43*, 7995−8048.
(6) (a) Olah, G. A.; Goeppert, A.; Prakash, S. G. K. *Beyond Oil and Gas: The Methanol Economy*, 2nd Ed.; Wiley-VCH: Weinheim, 2009. (b) Olah, G. A.; Prakash, S.G. K.; Goeppert, A. *J. Am. Chem. Soc.* **2011**, *133*, 12881−12898. (c) Olah, G. A. *Angew. Chem., Int. Ed.* **2013**, *52*, 104−107 and references therein..
(7) Thermochemical data have been calculated based on the Nist Chemistry Webbook at http://webbook.nist.gov/chemistry/.
(8) (a) Palo, D. R.; Dagle, R. A.; Holladay, J. D. *Chem. Rev.* **2007**, *107*, 3992−4021. (b) Sá, S.; Silva, H.; Brandão, L.; Sousa, J. M.; Mendes, A. *Appl. Catal., B* **2010**, *99*, 43−57.
(9) Nielsen, M.; Alberico, E.; Baumann, W.; Drexler, H.-J.; Junge, H.; Gladiali, S.; Beller, M. *Nature* **2013**, *495*, 85−89.
(10) (a) Bertoli, M.; Choualeb, A.; Lough, A. J.; Moore, B.; Spasyuk, D.; Gusev, D. G. *Organometallics* **2011**, *30*, 3479−3482. (b) Nielsen, M.; Kammer, A.; Cozzula, D.; Junge, H.; Gladiali, S.; Beller, M. *Angew. Chem., Int. Ed.* **2011**, *50*, 9593−9597. (c) Kuriyama, W.; Matsumoto, T.; Ino, Y.; Ogata, O. Takasago International Corporation, PCT Int. Appl. WO/2011/048727 A1, 2011. (d) Kuriyama, W.; Matsumoto, T.; Ogata, O.; Ino, Y.; Aoki, K.; Tanaka, S.; Ishida, K.; Kobayashi, T.; Sayo, N.; Saito, T. *Org. Process Res. Dev.* **2012**, *16*, 166−171.
(11) (a) Rodriguez-Lugo, R. E.; Trincado, M.; Vogt, M.; Tewes, F.; Santiso-Quinones, G.; Grützmacher, H. *Nat. Chem.* **2013**, *5*, 342−347. (b) Monney, A.; Barsch, E.; Sponholz, P.; Junge, H.; Ludwig, R.; Beller, M. *Chem. Commun.* **2014**, *50*, 707−709. (c) Hu, P.; Diskin-Posner, Y.; Ben-David, Y.; Milstein, D. *ACS Catal.* **2014**, *4*, 2649−2652. (d) Heim, L. E.; Thiel, D.; Gedig, C.; Deska, J.; Prechtl, M. H. G. *Angew. Chem., Int. Ed.* **2015**, *54*, 10308−10312.
(12) (a) Alberico, E.; Sponholz, P.; Cordes, C.; Nielsen, M.; Drexler, H.-J.; Baumann, W.; Junge, H.; Beller, M. *Angew. Chem., Int. Ed.* **2013**, *52*, 14162−14166. (b) Bielinski, E. A.; Förster, M.; Zhang, Y.; Bernskoetter, W. H.; Hazari, N.; Holthausen, M. C. *ACS Catal.* **2015**, *5*, 2404−2415.
(13) Selected references: (a) Gunanathan, C.; Milstein, D. *Chem. Rev.* **2014**, *114*, 12024−12087. (b) Annibale, V. T.; Song, D. *RSC Adv.* **2013**, *3*, 11432−11449. (c) Luca, O. R.; Crabtree, R. H. *Chem. Soc. Rev.* **2013**, *42*, 1440−1459. (d) Zhao, B.; Han, Z.; Ding, K. *Angew. Chem., Int. Ed.* **2013**, *52*, 4744−4788. (e) Schneider, S.; Meiners, J.; Askevold, B. *Eur. J. Inorg. Chem.* **2012**, *2012*, 412−429. (f) Lyaskovskyy, V.; de Bruin, B. *ACS Catal.* **2012**, *2*, 270−279. (g) Gunanathan, C.; Milstein, D. *Acc. Chem. Res.* **2011**, *44*, 588−602. (h) van der Vlugt, J. I.; Reek, J. N. H. *Angew. Chem., Int. Ed.* **2009**, *48*, 8832−8846.
(14) (a) Noyori, R.; Yamakawa, M.; Hashiguchi, S. *J. Org. Chem.* **2001**, *66*, 7931−7944. (b) Yamakawa, M.; Ito, H.; Noyori, R. *J. Am. Chem. Soc.* **2000**, *122*, 1466−1478. (c) Khusnutdinova, J. R.; Milstein, D. *Angew. Chem., Int. Ed.* **2015**, *54*, 12236−12273; *Angew. Chem.* **2015**, *127*, 12406−12445.
(15) Li, H.; Hall, M. B. *J. Am. Chem. Soc.* **2015**, *137*, 12330−12342.
(16) (a) Campos, J.; Sharninghausen, L. S.; Manas, M. G.; Crabtree, R. H. *Inorg. Chem.* **2015**, *54*, 5079−5084.
(17) Fujita, K.; Kawahara, R.; Aikawa, T.; Yamaguchi, R. *Angew. Chem., Int. Ed.* **2015**, *54*, 9057−9060.
(18) Handgraaf, J. W.; Meijer, E. J. *J. Am. Chem. Soc.* **2007**, *129*, 3099−3103.
(19) (a) Yang, X. *ACS Catal.* **2014**, *4*, 1129−1133. (b) Lei, M.; Pan, Y.; Ma, X. *Eur. J. Inorg. Chem.* **2015**, *2015*, 794−803.
(20) Blum, O.; Milstein, D. *J. Organomet. Chem.* **2000**, *593*−*594*, 479−484.
(21) (a) Kothandaraman, J.; Goeppert, A.; Czaun, M.; Olah, G. A.; Prakash, G. K. S. *J. Am. Chem. Soc.* **2016**, *138*, 778−781. (b) Kothandaraman, J.; Czaun, M.; Goeppert, A.; Haiges, R.; Jones, J.-P.; May, R. B.; Prakash, G. K. S.; Olah, G. A. *ChemSusChem* **2015**, *8*, 1442−1451. (c) Choi, J.-H.; Prechtl, M. H. *ChemCatChem* **2015**, *7*, 1023−1028. (d) Choi, J.-H.; Heim, L. E.; Ahrens, M.; Prechtl, M. H. G. *Dalton Trans* **2014**, *43*, 17248−17254. (e) Marziale, A. N.; Friedrich, A.; Klopsch, I.; Drees, M.; Celinski, V. R.; Schmedt auf der Günne, J.; Schneider, S. *J. Am. Chem. Soc.* **2013**, *135*, 13342−13355. (f) Han, Z.; Rong, L.; Wu, J.; Zhang, L.; Wang, Z.; Ding, K. *Angew. Chem., Int. Ed.* **2012**, *51*, 13041−13045. (g) Spasyuk, D.; Gusev, D. G. *Organometallics* **2012**, *31*, 5239−5242. (h) Zhang, L.; Raffa, G.; Nguyen, D. H.; Swesi, Y.; Corbel-Demailly, L.; Capet, F.; Trivelli, X.; Desset, S.; Paul, S.; Paul, J.-F.; Fongarland, P.; Dumeignil, F.; Gauvin, R. M. *J. Catal.* **2016**, *340*, 331−343.
(22) (a) Xu, R.; Chakraborty, S.; Bellows, S. M.; Yuan, H.; Cundari, T. R.; Jones, W. D. *ACS Catal.* **2016**, *6*, 2127−2135. (b) Zhang, Y.; MacIntosh, A. D.; Wong, J. L.; Bielinski, E. A.; Williard, P. G.; Mercado, B. Q.; Hazari, N.; Bernskoetter, W. H. *Chem. Sci.* **2015**, *6*, 4291−4299. (c) Bornschein, C.; Werkmeister, S.; Wendt, B.; Jiao, H.; Alberico, E.; Baumann, W.; Junge, H.; Junge, K.; Beller, M. *Nat. Commun.* **2014**, *5*, 4111. (d) Werkmeister, S.; Junge, K.; Wendt, B.; Alberico, E.; Jiao, H.; Baumann, W.; Junge, H.; Gallou, F.; Beller, M. *Angew. Chem., Int. Ed.* **2014**, *53*, 8722−8726. (e) Sharninghausen, L. S.; Mercado, B. Q.; Crabtree, R. H.; Hazari, N. *Chem. Commun.* **2015**, *51*, 16201−16204.
(23) (a) Jing, Y.; Chen, X.; Yang, X. *Organometallics* **2015**, *34*, 5716−5722. (b) Zhang, G.; Vasudevan, K. V.; Scott, B. L.; Hanson, S. K. *J. Am. Chem. Soc.* **2013**, *135*, 8668−8681. (c) Zhang, G.; Hanson, S. K. *Chem. Commun.* **2013**, *49*, 10151−10153. (d) Xu, R.; Chakraborty, S.; Yuan, H.; Jones, W. D. *ACS Catal.* **2015**, *5*, 6350−6354. (e) Zhang, G.; Yin, Z.; Tan, J. *RSC Adv.* **2016**, *6*, 22419−22423.
(24) Vasudevan, K. V.; Scott, B. L.; Hanson, S. K. *Eur. J. Inorg. Chem.* **2012**, *2012*, 4898−4906.
(25) Gómez-Gallego, M.; Sierra, M. A. *Chem. Rev.* **2011**, *111*, 4857−4963.
(26) Reactant molecules, methanol, and water, can effectively be removed from the rate equation. The catalyst and base concentration during the steady state period are also constant, making the kinetics effectively pseudo zero order, as exemplified by a constant rate of gas evolution in the short-to-medium term.
(27) (a) Sandoval, C. A.; Ohkuma, T.; Muñiz, K.; Noyori. *J. Am. Chem. Soc.* **2003**, *125*, 13490−13503. (b) Rautenstrauch, V.; Hoang-Cong, X.; Churlaud, R.; Abdur-Rashid, K.; Morris, R. H. *Chem. - Eur. J.* **2003**, *9*, 4954−4967. (c) Hamilton, R. J.; Bergens, S. H. *J. Am. Chem. Soc.* **2006**, *128*, 13700−13701. (d) Baratta, W.; Siega, K.; Rigo, P. *Chem. - Eur. J.* **2007**, *13*, 7479−7486. (e) Baratta, W.; Baldino, S.; Calhorda, M. J.; Costa, P. J.; Esposito, G.; Herdtweck, E.; Magnolia, S.; Mealli, C.; Messaoudi, A.; Mason, S. A.; Veiros, L. F. *Chem. - Eur. J.* **2014**, *20*, 13603−13617.
(28) The solid state structure of *anti*-**1a** has been recently reported: Zhang, L.; Nguyen, D. H.; Raffa, G.; Trivelli, X.; Capet, F.; Desset, S.; Paul, S.; Dumeignil, F.; Gauvin, R. M. *ChemSusChem* **2016**, *9*, 1413−1423.
(29) Despite exposure of the solid to high vacuum for a prolonged time, the ^{1}H NMR spectrum of **2** often contained a "*t*-Bu" peak from *t*-BuOH. A strong hydrogen bond between the alcohol, which is too bulky to add across the Ru—N amido bond, and **2** may explain these observations. See Prokopchuk, E. D.; Tsui, B. T. H.; Lough, A. J.; Morris, R. H. *Chem. - Eur. J.* **2014**, *20*, 16960−16968.
(30) A related amido complex, bearing a PMe_3 in place of CO has been reported by Schneider that shows similar structural features: Friedrich, A.; Drees, M.; Käss, M.; Herdtweck, E.; Schneider, S. *Inorg. Chem.* **2010**, *49*, 5482−5494.
(31) Jordan, R. B. *Reaction Mechanisms of Inorganic and Organometallic Systems*, 3rd Ed., Oxford University Press: Oxford, U.K., 2007.
(32) The remaining 10% of the total Ru content is due to minor monohydride species, among which two were more abundant (^{1}H NMR (THF-d_8): δ−18.09 (t, J_{HP} = 17.8 Hz) and ^{31}P{^{1}H} NMR: δ =

DOI: 10.1021/jacs.6b05692
J. Am. Chem. Soc. 2016, 138, 14890−14904

78.6 (s); ^{1}H NMR (THF-d_8): δ −18.58 (t, J_{HP} = 17.5 Hz) and ^{31}P{^{1}H} NMR: δ = 76.9 (s)).
(33) (a) Buckingham, A. D.; Stephens, P. J. *J. Chem. Soc.* **1964**, 2747−2759. (b) Appleton, T. G.; Clark, H. C.; Manzer, L. E. *Coord. Chem. Rev.* **1973**, *10*, 335−422.
(34) (a) Koike, T.; Ikariya, T. *Organometallics* **2005**, *24*, 724−730. (b) Hamilton, R. J.; Bergens, S. H. *J. Am. Chem. Soc.* **2008**, *130*, 11979−11987. (c) Takebayashi, S.; Dabral, N.; Miskolzie, M.; Bergens, S. H. *J. Am. Chem. Soc.* **2011**, *133*, 9666−9669.
(35) (a) Bryndza, H. E.; Tam, W. *Chem. Rev.* **1988**, *88*, 1163−1188. (b) Fulton, J. R.; Holland, A. W.; Fox, D. J.; Bergman, R. G. *Acc. Chem. Res.* **2002**, *35*, 44−56.
(36) Traces of protic solvent must provide the required proton for the formation of **3**.
(37) The molecular structure of a similar Ru carbonate complex bearing the diphenyl substituted PNP ligand has been reported. See ref 21b.
(38) For example: (a) Prokopchuk, D. E.; Collado, A.; Lough, A. J.; Morris, R. H. *Dalton Trans.* **2013**, *42*, 10214−10220. (b) Kohl, S. W.; Weiner, L.; Schwartsburd, L.; Konstantinovski, L.; Shimon, L. J. W.; Ben-David, Y.; Iron, M. A.; Milstein, D. *Science* **2009**, *324*, 74−77.
(39) (a) Grasemann, M.; Laurenczy, G. *Energy Environ. Sci.* **2012**, *5*, 8171−8181. (b) Beller, M.; Bornscheuer, U. T. *Angew. Chem., Int. Ed.* **2014**, *53*, 4527−4528. (c) Wang, W.-H.; Himeda, Y.; Muckerman, J. T.; Manbeck, G. F.; Fujita, E. *Chem. Rev.* **2015**, *115*, 12936−12973.
(40) CO_2 hydrogenation: (a) Filonenko, G. A.; van Putten, R.; Schulpen, E. N.; Hensen, E. J. M.; Pidko, E. A. *ChemCatChem* **2014**, *6*, 1526−1530. (b) Filonenko, G. A.; Conley, M. P.; Coperet, C.; Lutz, M.; Hensen, E. J. M.; Pidko, E. A. *ACS Catal.* **2013**, *3*, 2522−2526. (c) Huff, C. A.; Sanford, M. S. *ACS Catal.* **2013**, *3*, 2412−2416. (d) Hull, J. F.; Himeda, Y.; Wang, W.-H.; Hashiguchi, B.; Periana, R.; Szalda, D. J.; Muckerman, J. T.; Fujita, E. *Nat. Chem.* **2012**, *4*, 383−388. (e) Schmeier, T. J.; Dobereiner, G. E.; Crabtree, R. H.; Hazari, N. *J. Am. Chem. Soc.* **2011**, *133*, 9274−9277. (f) Langer, R.; Diskin-Posner, Y.; Leitus, G.; Shimon, L. J. W.; Ben-David, Y.; Milstein, D. *Angew. Chem., Int. Ed.* **2011**, *50*, 9948−9952. (g) Yamashita, M.; Nozaki, K. *J. Am. Chem. Soc.* **2009**, *131*, 14168−14169. HCOOH dehydrogenation: (h) Bielinski, E. A.; Lagaditis, P. O.; Zhang, Y.; Mercado, B. Q.; Würtele, C.; Bernskoetter, W. H.; Hazari, N.; Schneider, S. *J. Am. Chem. Soc.* **2014**, *136*, 10234−10237. (i) Zell, T.; Butschke, B.; Ben-David, Y.; Milstein, D. *Chem. - Eur. J.* **2013**, *19*, 8068−8072. (l) Tanaka, R.; Yamashita, M.; Chung, L. W.; Morokuma, K.; Nozaki, K. *Organometallics* **2011**, *30*, 6742−6750.
(41) Steiner, T. *Angew. Chem., Int. Ed.* **2002**, *41*, 48−76.
(42) (a) Crabtree, R. H. *Chem. Rev.* **2016**, *116*, 8750−8769. (b) Abdur-Rashid, K.; Clapham, S. E.; Hadzovic, A.; Harvey, J. N.; Lough, A. J.; Morris, R. H. *J. Am. Chem. Soc.* **2002**, *124*, 15104−15118. (c) Field, L. D.; Hambley, T. W.; Yau, B. C. K. *Inorg. Chem.* **1994**, *33*, 2009−2017.
(43) (a) Pitman, C. L.; Brereton, K. R.; Miller, A. J. M. *J. Am. Chem. Soc.* **2016**, *138*, 2252−2260. (b) Bullock, R. M.; Appel, A. M.; Helm, M. L. *Chem. Commun.* **2014**, *50*, 3125−3143. (c) Jacobsen, H.; Berke, H. *Recent Advances in Hydride Chemistry*; Peruzzini, M., Poli, R., Eds.; Elsevier: Amsterdam, 2001; pp 89−116.
(44) Decoupling from phosphorus in the ^{1}H{^{31}P} NMR spectrum resolved the multiplet into two well-resolved doublets, with only the residual $^{2}J_{H-H}$ coupling remaining for each hydride.
(45) (a) Belkova, N. V.; Epstein, L. M.; Shubina, E. S. *Eur. J. Inorg. Chem.* **2010**, *2010*, 3555−3565. (b) Bakhmutov, V. I. *Eur. J. Inorg. Chem.* **2005**, *2005*, 245−255. (c) Custelcean, R.; Jackson, J. E. *Chem. Rev.* **2001**, *101*, 1963−1980.
(46) Friedrich, A.; Drees, M.; auf der Günne, J. S.; Schneider, S. *J. Am. Chem. Soc.* **2009**, *131*, 17552−17553.
(47) Käss, M.; Friedrich, A.; Schneider, S. *Angew. Chem., Int. Ed.* **2009**, *48*, 905−907.
(48) Due to fast equilibration, the HCO_3^-/CO_3^- anions gave rise to a single ^{13}C NMR peak, the chemical shift of which depends on their relative concentration and therefore on the pH. See: (a) Moret, S.; Dyson, P. J.; Laurenczy, G. *Dalton Trans.* **2013**, *42*, 4353−4356. (b) Mani, F.; Peruzzini, M.; Stoppioni, P. *Green Chem.* **2006**, *8*, 995−1000.
(49) (a) Dub, P. A.; Henson, N. J.; Martin, R. L.; Gordon, J. C. *J. Am. Chem. Soc.* **2014**, *136*, 3505−3521. (b) Hartmann, R.; Chen, P. *Angew. Chem., Int. Ed.* **2001**, *40*, 3581−3585.
(50) John, J. M.; Takebayashi, S.; Dabral, N.; Miskolzie, M.; Bergens, S. H. *J. Am. Chem. Soc.* **2013**, *135*, 8578−8584.
(51) The proton affinity (PA) of each complex was calculated and compared to a calibration curve that was populated with known pK_as and calculated PAs.
(52) (a) Kapoor, S.; Barnabas, F. A.; Sauer, M. C., Jr.; Meisel, D.; Jonah, C. D. *J. Phys. Chem.* **1995**, *99*, 6857−6863. (b) Ashby, E. C.; Doctorovich, F.; Liotta, C. L.; Neumann, H. M.; Barefield, E. K.; Konda, A.; Zhang, K.; Hurley, J. *J. Am. Chem. Soc.* **1993**, *115*, 1171−1173.
(53) Besora, M.; Lledós, A.; Maseras, F. *Chem. Soc. Rev.* **2009**, *38*, 957−966.
(54) Examples of hemilability at the side donor sites of pincer ligands: (a) Canovese, L.; Visentin, F.; Chessa, G.; Uguagliati, P.; Santo, C.; Bandoli, G.; Maini, L. *Organometallics* **2003**, *22*, 3230−3238. (b) Bassetti, M.; Capone, A.; Salamone, M. *Organometallics* **2004**, *23*, 247−252. (c) Zhang, J.; Leitus, G.; Ben-David, Y.; Milstein, D. *J. Am. Chem. Soc.* **2005**, *127*, 10840−10841. (d) Choualeb, A.; Lough, A. J.; Gusev, D. G. *Organometallics* **2007**, *26*, 5224−5229. (e) Vuzman, D.; Poverenov, E.; Shimon, L. J. W.; Diskin-Posner, Y.; Milstein, D. *Organometallics* **2008**, *27*, 2627−2634. (f) Fulmer, G. R.; Kaminsky, W.; Kemp, R. A.; Goldberg, K. I. *Organometallics* **2011**, *30*, 1627−1636. (g) Lindner, R.; van den Bosch, B.; Lutz, M.; Reek, J. N. H.; van der Vlugt, J. I. *Organometallics* **2011**, *30*, 499−510. (h) Ruddy, A. J.; Mitton, S. J.; McDonald, R.; Turculet, L. *Chem. Commun.* **2012**, *48*, 1159−1161.
(55) Examples of hemilability at the central donor site of the pincer ligand: (a) Bernhammer, J. C.; Frison, G.; Huynh, H. V. *Dalton Trans.* **2014**, *43*, 8591−8594. (b) Zhao, C.; Jennings, M. C.; Puddephatt, R. J. *Dalton Trans.* **2008**, 1243−1250. (c) Moxham, G. L.; Randell-Sly, H.; Brayshaw, S. K.; Weller, A. S.; Willis, M. C. *Chem. - Eur. J.* **2008**, *14*, 8383−8397. (d) Moxham, G. L.; Randell-Sly, H. E.; Brayshaw, S. K.; Woodward, R. L.; Weller, A. S.; Willis, M. C. *Angew. Chem., Int. Ed.* **2006**, *45*, 7618−7622.
(56) N-alkylation of amine ligands is known to decrease the stability constants of their metal ion complexes: Meyerstein, D. *Coord. Chem. Rev.* **1999**, *185*−*186*, 141−147.
(57) (a) Smythe, N. A.; Grice, K. A.; Williams, B. S.; Goldberg, K. I. *Organometallics* **2009**, *28*, 277−288. (b) Fafard, C. M.; Ozerov, O. V. *Inorg. Chim. Acta* **2007**, *360*, 286−292.

DOI: 10.1021/jacs.6b05692
J. Am. Chem. Soc. 2016, 138, 14890−14904